compartmental model for the brain to the heart is not permitted, because subtraction for spillover from gas volume in addition to that from the blood pool is needed. A previous study demonstrated that the gas volume can be accurately estimated from the transmission scan data; thus, this technique did not require additional emission scanning for estimating the quantitative gas volume images [6, 7]. However, gaseous radioactivity in the lung during the inhalation of ^{15}O-O_2 gas is too high in comparison to other regions. Subtraction for this contribution is straightforward and accurate using the transmission scan-derived gaseous volume images, but the lung radioactivity degraded image quality in the estimated $MMRO_2$ images.

As an alternative to gas inhalation, we recently developed a method to prepare an injectable form of ^{15}O-O_2. This was accomplished by exposing pre-collected blood to ^{15}O-O_2 gas using a small artificial lung system resulting in a maximum yield of 130 MBq/ml. We demonstrated that cerebral oxygen metabolism could be estimated in normal and ischemic rats using injectable ^{15}O-O_2 [10–12]. This technique has the potential of avoiding the inhalation protocol.

The aim of the present study was therefore to test the feasibility of using the injectable ^{15}O-O_2 oxygen system for estimating myocardial oxygen metabolism in pigs. The injection method was compared to the inhalation method to determine if the injection method resulted in a reduction of lung radioactivity, an improved image quality, a more accurate estimate of myocardial oxygen metabolism, and an improved signal-to-noise ratio.

Materials and methods

Theory

^{15}O-Oxygen was administered by IV injection or inhalation and was carried as ^{15}O-hemoglobin by blood to peripheral tissues including the myocardium, where it was converted to ^{15}O-water (^{15}O-H_2O_{met}) through aerobic metabolism. The increased distribution volume of ^{15}O-H_2O_{met}, represented by the exchangeable water space of tissue, causes delayed removal of radioactivity. This allows the definition of an appropriate model and equations to be derived for the calculation of a regional myocardial metabolic rate for oxygen ($rMMOR_2$) and regional oxygen extraction fraction (rOEF). Previous studies demonstrated that these calculations were similar to those used for estimating cerebral blood flow and oxygen metabolism and require the measurement of regional myocardial blood flow (rMBF) and a correction for spillover of activity from the vascular pools and the pulmonary alveoli [6, 7]. rMBF was measured by the ^{15}O-H_2O injection technique [13]. Activity in the vascular pools of the heart chambers and the lung was evaluated with a conventional measurement of blood volume using ^{15}O-CO, and activity in the pulmonary alveoli was evaluated with an unconventional and indirect measurement of gas volume obtained from the transmission scan. Furthermore, the existence of recirculating ^{15}O-H_2O_{met} in the blood freely accessible to the myocardium was taken into consideration.

The differential equation describing the myocardial kinetics after administration of ^{15}O-O_2 can be written as follows:

$$\frac{dC^{myo}(t)}{dt} = OEF \cdot f \cdot A_o(t) + f \cdot A_w(t) - \left(\frac{f}{p} + \lambda\right) C^{myo}(t) \quad (1)$$

where $C^{myo}(t)$ designates the true radioactivity concentration in the myocardium at time t, f is myocardial blood flow, $A_O(t)$ is the ^{15}O-O_2 radioactivity concentration in arterial blood, $A_W(t)$ is the ^{15}O-H_2O radioactivity concentration in arterial blood, p is the myocardium/blood partition coefficient of water, and λ is the physical decay constant of O-15.

Solving Eq. (1) in terms of $C^{myo}(t)$ gives:

$$C^{myo}(t) = OEF \cdot f \cdot A_o(t) * e^{-\left(\frac{f}{p}+\lambda\right)\cdot t} + f \cdot A_w(t) * e^{-\left(\frac{f}{p}+\lambda\right)\cdot t} \quad (2)$$

where the asterisk denotes the convolution integral. During steady-state conditions under the continuous administration of ^{15}O-O_2, the following relationship holds:

$$C^{myo} = \frac{OEF \cdot f \cdot A_o + f \cdot A_w}{\left(\frac{f}{p} + \lambda\right)} \quad (3)$$

In the actual PET studies, the spillover from vascular pools and pulmonary alveoli and the partial volume effect should be taken into consideration [14]. Then, the measured radioactivity concentration in the region of interest (ROI) in the myocardium ($R^{myo}(t)$) can be expressed as:

$$\begin{aligned} R^{myo}(t) = {} & \alpha \cdot C^{myo}(t) \\ & + (V_B^{myo} \cdot A_t(t) - \alpha \cdot F_{Vein} \cdot OEF \cdot A_o(t) - \alpha \cdot F_{Vein} \cdot A_w(t)) \\ & + V_G^{myo} \cdot C_{gas}(t) \end{aligned} \quad (4)$$

where α denotes the myocardial tissue fraction, V_B^{myo} is the myocardial blood volume, $A_t(t)$ is the total O-15 radioactivity concentration in arterial blood, F_{vein} is the microscopic venous blood volume, V_G^{myo} is the gas volume in the myocardial ROI and $C_{gas}(t)$ is the O-15 radioactivity concentration in V_G^{myo}.

With the bolus injection or infusion methods using an artificial lung system, the radioactivity in the pulmonary alveoli is expected to be negligible in comparison with the inhalation method. Thus, Eq. (4) can be converted to:

$$R^{myo}(t) = \alpha \cdot C^{myo}(t) + (V_B^{myo} \cdot A_t(t) - \alpha \cdot F_{Vein} \cdot OEF \cdot A_o(t) - \alpha \cdot F_{Vein} \cdot A_w(t)) \quad (5)$$

Subjects

In this study, four healthy miniature pigs (22–30 kg) were used. The pigs were anesthetized by IM injection of ketamine and xylazine followed by continuous infusion of propofol (5 mg/kg/h). The animals were then placed in the supine position on the bed of the PET scanner. All experimental procedures were approved by the local animal welfare committee.

Injectable ^{15}O-O_2 preparation

In the "injection" study, injectable ^{15}O-O_2 was used. Injectable ^{15}O-O_2 was prepared as described previously [10–12]. In brief, part of an infusion line kit (Terumo Corporation, Tokyo, Japan) and an artificial lung 18 cm in length (Senko Medical Instrument Mfg Co. Ltd., Tokyo, Japan) were connected using silicone tubing to make a closed system. Then, venous blood collected from a pig, which was used in the following PET studies, was added to the system and circulated (100 ml/min) by a peristaltic pump, followed by introduction of ^{15}O–O_2 gas (~7,000 MBq/min/433 ml) into the artificial lung for 15 min to prepare injectable ^{15}O-O_2 (5.6–60.7 MBq/ml).

In the "continuous infusion" study, the left femoral artery and right femoral vein were both cannulated. The two cannulas from the artery and the vein were connected to the opposite sides of an artificial lung to create a femoral shunt. The blood flow in the shunt was aided by a peristaltic pump (30–50 ml/min). ^{15}O-O_2 gas (~7,000 MBq/min/433 ml) was continuously introduced into the artificial lung.

PET protocol (Fig. 1)

The PET scanner was an ECAT EXACT HR (CTI/Siemens) [15], which has an imaging field of view (FOV) of 55 cm in diameter and 15 cm in axial length. The spatial resolution of the scanner is 5.8 mm in full width at half maximum at the center of the FOV.

After obtaining a 20-min transmission scan for attenuation correction and gas volume estimation, the blood pool image was obtained with a 4-min PET scan after the pigs inhaled 2.7 GBq ^{15}O-CO for 30 s. Arterial blood samples were taken every minute during the ^{15}O-CO scanning, and

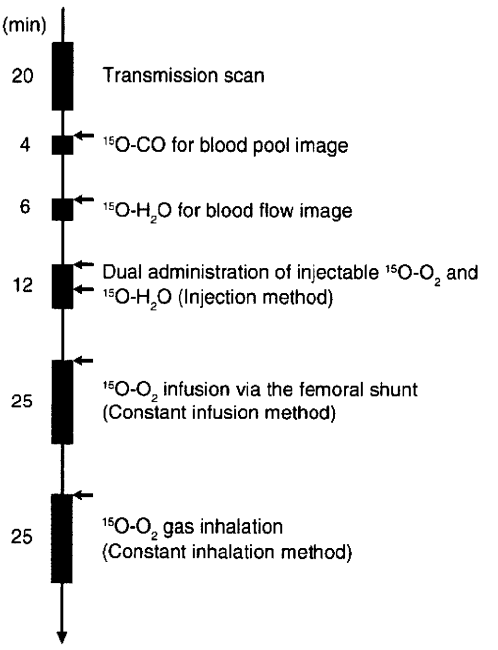

Fig. 1 Outline of the PET imaging study. The interval between scans was more than 15 min to allow for physical decay of O-15 radioactivity to background levels

the radioactivity concentration in the whole blood was measured with a NaI well-type scintillation counter calibrated against the PET scanner. Subsequently, ^{15}O-water was injected into the right femoral vein for 30 s at an infusion rate of 10 ml/min (injected radioactivity was about 1.11 GBq). Immediately after injection of ^{15}O-water, 26 dynamic frames (12×5 s, 8×15 s and 6×30 s) of PET data were acquired for 6 min.

Furthermore, two PET scans were successively performed after the IV injection of ^{15}O-O_2 (5.6–60.7 MBq/ml) for 30 s at an injection rate of 20–80 ml/min for the "injection" study, and by the continuous ^{15}O-O_2 gas infusion through the artificial lung in the femoral shunt for the "continuous infusion" study. In the "injection" study, 52 dynamic frames (12×5 s, 8×15 s, 6×30 s, 12×5 s, 8×15 s and 6×30 s) of PET data were acquired for 12 min, and 1.11 GBq of ^{15}O-water was injected IV for 30 s at 10 ml/min starting at 6 min after the administration of IV ^{15}O-O_2 according to the dual administration protocol we developed previously [16]. In the "continuous infusion" study, 26 dynamic frames (10×30 s, 5×60 s, 1×600 s and 10×30 s) were acquired for 25 min, and the 600-s frame was used for steady-state analysis.

Another PET scan was performed by ^{15}O-O_2 gas inhalation in one of the four pigs in the same protocol as the "continuous infusion" study. This was the "continuous inhalation" study. The interval between scans was more

than 15 min to allow for physical decay of O-15 radioactivity to background levels. All acquisitions were obtained in the two-dimensional mode (septa extended).

Data analysis

A filtered back-projection algorithm with a 6-mm Gaussian filter was used for image reconstruction. The reconstructed images had a matrix size of 128 × 128 × 47 and a voxel size of 1.84 × 1.84 × 3.38 mm, and all image data sets were resliced into short-axis images across the left ventricle [13].

Myocardial blood flow

rMBF was calculated from the injection of ^{15}O-H_2O by fitting the myocardial and arterial time-activity curve data to a single-tissue-compartment model that implemented corrections for partial-volume effects by introducing the tissue fraction. In addition, the model was corrected for spillover from the left ventricular (LV) chamber into the myocardial ROI by introducing the arterial blood volume [13]. In these experiments, the time-activity curves generated from large ROIs placed in the LV chamber were used as the input function.

Regional oxygen extraction fraction

In the "injection" study, rOEF was calculated according to Eqs. (2) and (5). In these formulations, F_{vein} was assumed to be 0.10 ml/g tissue and p was fixed at 0.90 ml/g. The blood volume image obtained from the ^{15}O-CO scan was used for the determination of V_B^{myo}. The value of $A_t(t)$ was obtained from the LV radioactivity concentration measured from the PET data set with small LV ROIs to minimize spillover from the myocardium. The calculation for the estimation of recirculating ^{15}O-H_2O was performed as previously described [16]. For the "continuous infusion" and "continuous inhalation" studies, in which a 600-s frame was regarded as steady-state, Eqs. (3) and (5) or Eqs. (3) and (4) were used for calculating rOEF, respectively.

Results

Table 1 summarizes the conditions of animals during the PET studies. The parameters were all within the physiologic range.

Figure 2 demonstrates the dynamic images obtained in the "injection", "continuous infusion", and "continuous inhalation" studies. With the injection and continuous-infusion methods, the right ventricle on the left side and the vena cava on the lower side were well delineated, whereas the left ventricle was moderately shown on the right side. The 16th frame (600~1,200 s after the initiation), which was used for steady-state analysis with the continuous-infusion method, was visibly distinct compared with all of the frames obtained with the injection method. However, with the continuous-inhalation method, neither ventricle could be depicted because of high radioactivity in the lung on the right and lower-side images.

The radioactivity in the blood pool obtained by ^{15}O-CO PET (Fig. 3g) and the gaseous volume estimated by inverse transmission data (Fig. 3h) were subtracted from the raw PET images (16th frame) with the continuous-inhalation and continuous-infusion methods, respectively (Fig. 3e and f). Both methods clearly delineated the myocardium after subtraction in comparison to the blood flow image (Fig. 3i). However, the continuous-inhalation method showed salient radioactivity on the lateral wall (Fig. 3e), whereas the continuous-infusion method showed only modest radioactivity in the myocardium (Fig. 3f). It is also notable that there was considerable radioactivity in the right ventricle with the continuous-infusion method even after the subtraction (Fig. 3f).

To further examine the differences between the continuous-infusion and continuous-inhalation methods, time-radioactivity curves during the PET scans were taken from four ROIs: the left ventricle (LV), right ventricle (RV), myocardium (Myo), and lung (Fig. 4). At the steady-state frame (600~1,200 s), the continuous-infusion method showed higher radioactivity in the RV and LV than in the myocardium (Fig. 4a), whereas the radioactivity of these regions was similar with the continuous-inhalation method (Fig. 4b). The radioactivity in LV was about two-thirds of that in RV in Fig. 4a, indicating that measurable radioactivity was excreted through the lung even after the femoral administration of ^{15}O-O_2. The lung excretion was also observed on the blood-subtracted image (Fig. 3e). Actually, there was significant radioactivity in the lung (Fig. 4a), although that was the lowest among the four ROIs. In contrast, the radioactivity in the myocardium was the lowest among the four ROIs with the continuous-inhalation method

Table 1 Physiological parameters of pigs during the PET studies

	pH	pCO_2 (mmHg)	pO_2 (mmHg)	tHb (g/dl)	O_2Sat (%)	HR (bpm)	BP (mmHg)	
							Diastolic	Systolic
Average	7.46	40.3	125.8	12.8	97.7	85	97.8	125.2
SD	0.032	2.51	16.69	1.30	1.83	19.5	10.4	19.3

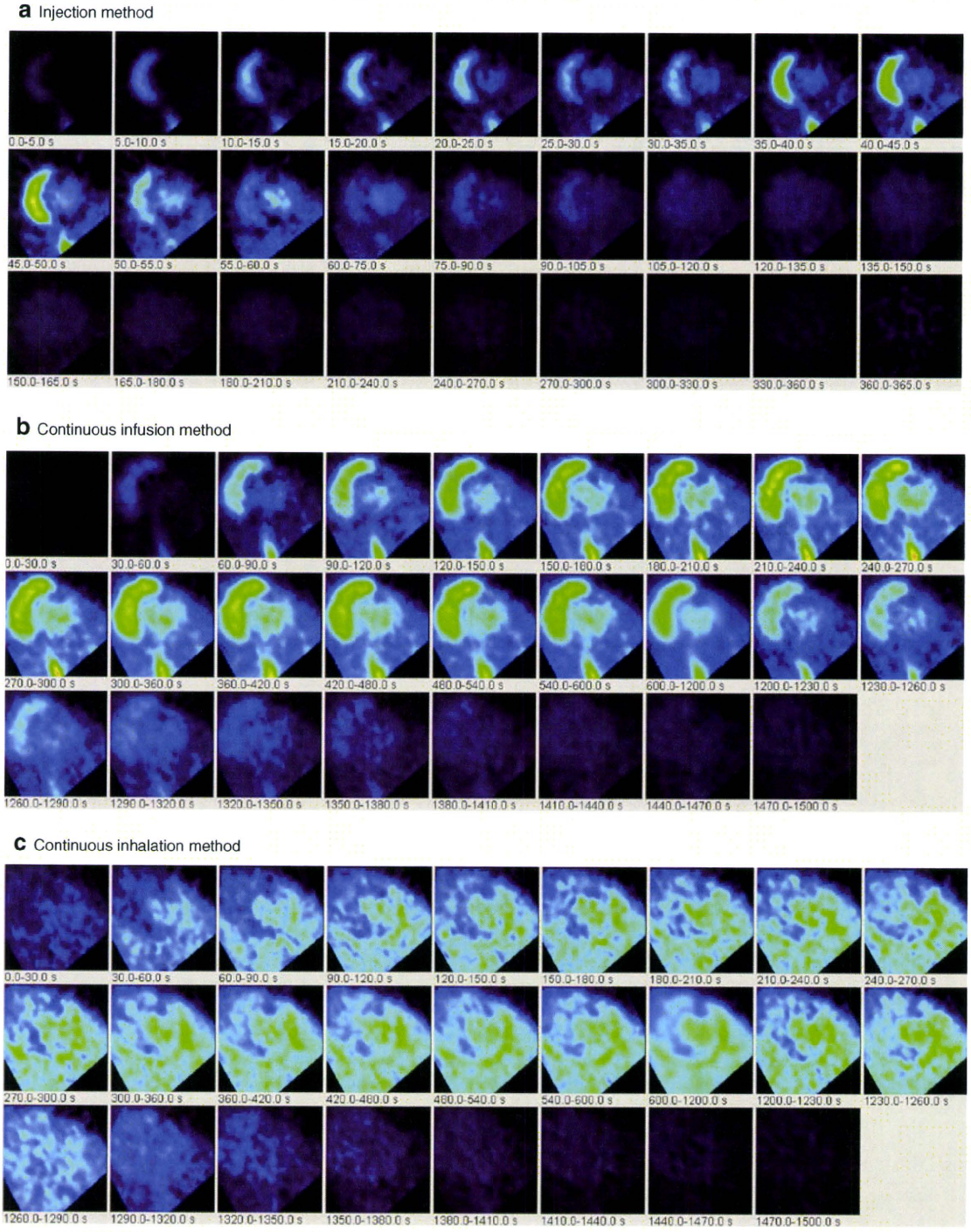

Fig. 2 PET images obtained in (**a**) the injection method, (**b**) the continuous-infusion method with injectable ^{15}O-O_2, and (**c**) the continuous-inhalation method with ^{15}O-O_2 gas

(Fig. 4b). The heart-to-lung radioactivity ratios were calculated from Fig. 4 for the quantitative estimation of image quality; the continuous-infusion method provided a ratio of 1.38±0.24, whereas the ratio was less than one with the continuous-inhalation method.

Table 2 shows the quantitative OEF values in the lateral wall obtained by the injection, continuous-infusion, and continuous-inhalation methods. These OEF values were consistent among the three methods.

Figure 5 represents the noise equivalent counts (NEC) standardized by the total counts detected by the PET scanner. Although the injection method tended to show rather high values, there was no significant difference between the values obtained by the injection and

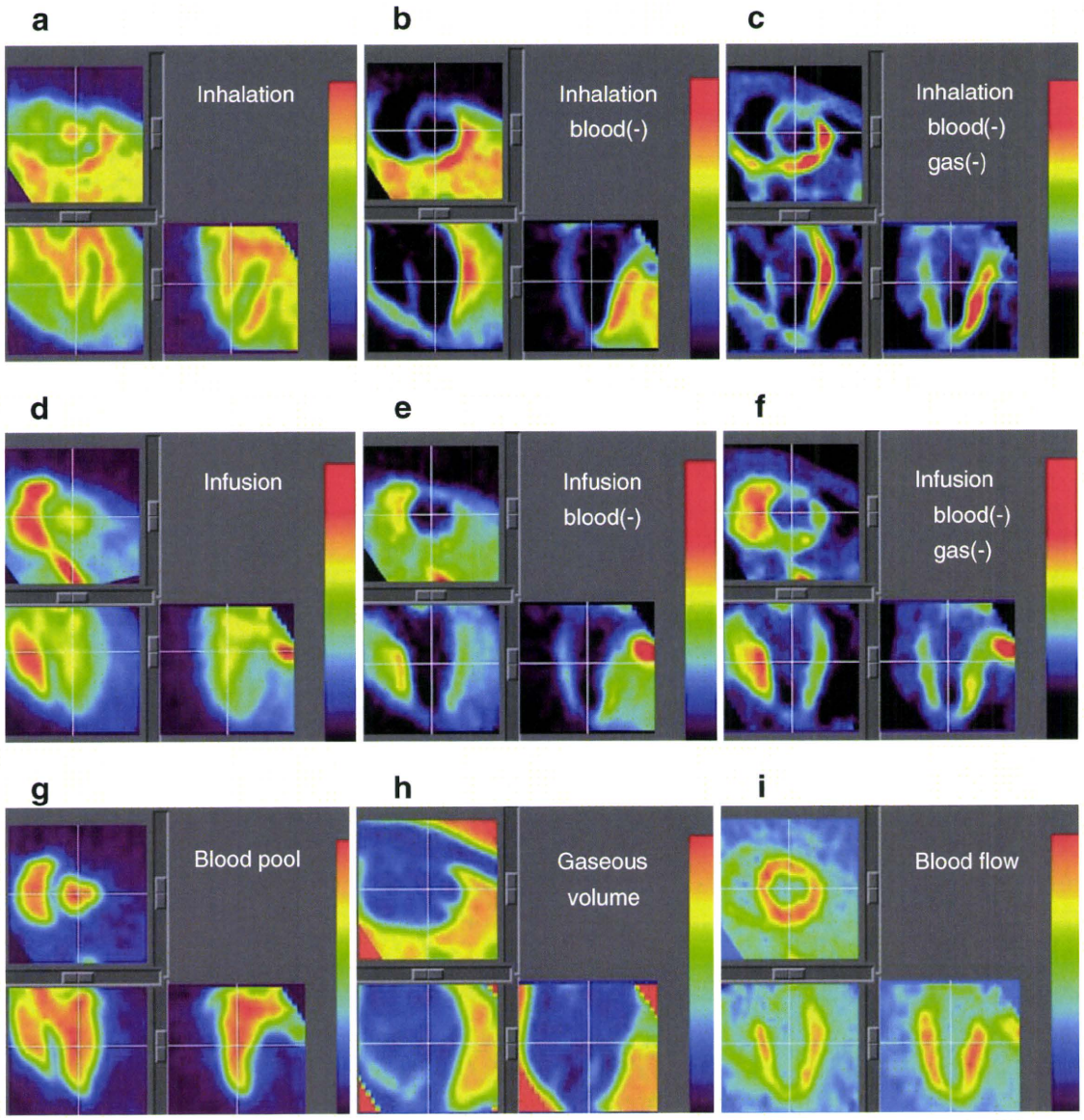

Fig. 3 PET images obtained in the study are shown. The 16th frame (steady-state frames) of the continuous-inhalation method and the continuous-infusion method are shown in (**a**) and (**d**), respectively. The 'blood-subtracted' images shown in (**b**) and (**e**) were created by subtraction of the blood-pool image by ^{15}O-CO (**g**) from (**a**) and (**d**). The 'blood- and gas-subtracted' images shown in (**c**) and (**f**) were created by the successive subtraction of the gaseous image (**h**) from (**b**) and (**e**). The myocardial blood flow image is also shown in (**i**)

continuous-infusion methods as determined by a Mann Whitney *U*-test.

Discussion

In previous studies, we showed the usefulness of the injectable ^{15}O-O_2 system for estimating cerebral oxygen metabolism in small animals such as rats under normal or ischemic conditions [10–12]. Injectable ^{15}O-O_2 replaced the inhalation protocol and radioactive ^{15}O-O_2 was administered via the tail vein. Thus, injectable ^{15}O-O_2 could abolish the artifact from the high radioactivity in the inhalation tube that distorts the PET images, especially in small animals. We considered that the concept could also be utilized in the hearts of large animals. Therefore, in the present study, we tested the feasibility of an injectable ^{15}O-O_2 system for estimating myocardial oxygen metabolism in normal pigs. In addition, since a shunt between the femoral artery and vein can be created in pigs but not in small animals, continuous infusion via the femoral shunt was also performed to achieve a constant and reliable delivery of radioactivity to the heart.

Dynamic PET scans showed a large difference in the radioactivity distribution among the three methods. Since the labeling efficiency to prepare injectable ^{15}O-O_2 was

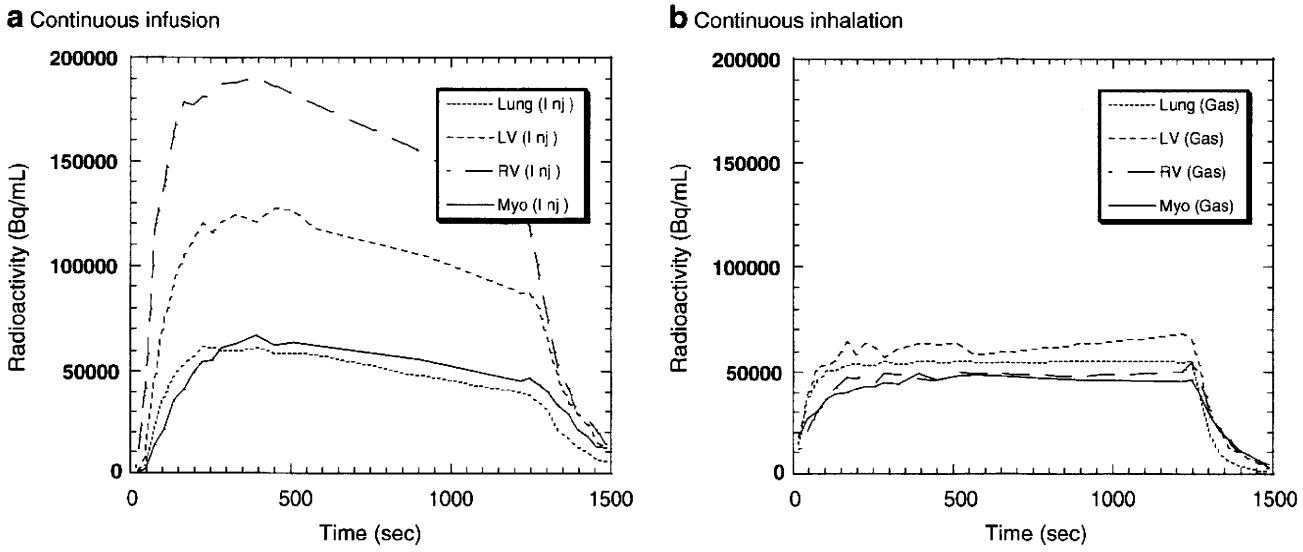

Fig. 4 Time-activity curves from the left ventricle (*LV*), the right ventricle (*RV*), the myocardium (lateral wall, Myo) and a lung region with the continuous-infusion method (**a**) and the continuous-inhalation method (**b**). The supply of radioactivity was started at time 0 s and stopped at 1,200 s. The 16th frame for the steady-state analysis was 600–1,200 s

lower with pig blood (ca. 61 MBq/ml at most) than with the blood of rats and humans (130 MBq/ml), the injection method provided rather obscure images. With the injection and continuous-infusion methods, the radioactivity in the lung was dramatically reduced in comparison to the continuous-inhalation method, since the heart-to-lung ratio with the continuous-infusion method was about 40% higher than with the continuous-inhalation method. This finding suggested that the two methods that inject radioactivity via a vein are more useful for analyzing myocardial oxygen metabolism in pigs than the continuous-inhalation method. However, a distinct difference between radioactivity of the right and left ventricles was observed in the images and time-radioactivity curves after venous administration of ^{15}O-O_2, indicating a certain degree of excretion of the radioactivity by the lung. Therefore, the spillover from the pulmonary alveoli to the myocardium could not be omitted in the two methods with venous administration, and Eq. (4) was used for the OEF analysis, although the radioactivity in the lung was lower than that in the myocardium.

On the other hand, with the continuous-inhalation method, the radioactivity of the lung was in between the radioactivity in the RV and LV. This is curious because O-15 radioactivity was supplied from the inhalation tube and transferred from the lung to blood so that the radioactivity in the lung should have been the highest among the four ROIs. This may have been caused, in part, by inhomogeneous distribution of the radioactivity in the lung due to its structure in comparison with the myocardium and ventricles, and/or by artifacts from the lung to other

Table 2 OEF estimated by the three methods using injectable ^{15}O-O_2 or ^{15}O-O_2 gas

	OEF		
	Injection	Infusion	Inhalation
Pig. 1	0.70	0.72	
Pig. 2	0.67	0.72	
Pig. 3	0.71	0.74	
Pig. 4	0.76	0.69	0.72
Average	0.71	0.72	0.72
SD	0.036	0.020	

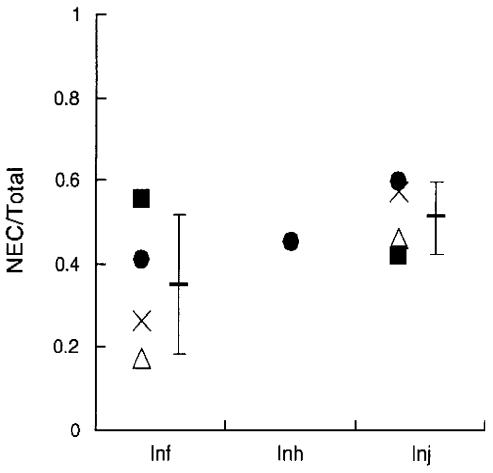

Fig. 5 The ratio of noise equivalent counts (*NEC*) to total counts in the total field of view of the PET scanner obtained with the continuous-infusion method (*Inf*), the continuous-inhalation method (*Inh*) and the injection method (*Inj*)

tissues. In any case, it is notable that the radioactivity in the myocardium was the lowest with the continuous-inhalation method, leading to difficulty in analyzing myocardial oxygen metabolism.

The OEF values in lateral walls were calculated to compare the ability of the three methods to determine myocardial oxygen metabolism by using the blood flow derived from the dual-administration protocol with the injection method and the single-administration protocol with the two continuous methods. There was no difference in the blood flow between the two protocols. Consequently, the three methods provided the same OEF value of about 0.7 and this is a physiological value in normal pigs, as was previously demonstrated [17, 18]. We have demonstrated the potential of the injectable ^{15}O-O_2 system for the estimation of physiological cerebral oxygen metabolism in rats and monkeys during early and late ischemia, hypertension, and ischemia plus hypertension [10–12, 19]. Therefore, we believe that the injection and continuous-infusion methods provide a physiological OEF in the myocardium. Nevertheless, we recognize the necessity to evaluate the reliability and usefulness of the injectable ^{15}O-O_2 method in myocardial applications. Further studies using pathophysiological animal models are required in the future, such as myocardial ischemia, hypoxia, and heart failure. On the other hand, since $MMRO_2$ is basically regarded as the product of MBF and OEF, the results indicated that these three methods were equivalent in their ability to quantify $MMRO_2$ in normal pigs, at least in the lateral wall. Although the images after the subtraction of spillovers from blood and gas showed different contrast between the continuous-infusion and continuous-inhalation methods, the ability of these two methods to measure OEF and $MMRO_2$ in the lateral walls was equivalent.

We did not evaluate myocardial oxygen metabolism in other heart regions since the radioactivity in the right ventricle could not be removed due to a significant difference of radioactivity between the ventricles with the continuous-infusion method. The injection method might be able to evaluate oxygen metabolism in other regions besides the lateral wall, although this was not evaluated in this study due to the low radioactivity of injectable ^{15}O-O_2 as described above. In the injection method, O-15 radioactivity was delivered from the femoral vein to RV, the lung, LV, and finally the myocardium. Thus, when the LV and myocardial activity reach a maximum, the RV activity is expected to be low. The later frames of the dynamic PET images with the injection method might avoid the high RV activity and delineate the myocardium and LV more clearly. With accurate anatomical information by gated PET/CT, the injection method will provide oxygen metabolism in other heart regions. In addition, the injection method has a benefit in that it is noninvasive and shortens the acquisition time in comparison with the continuous-infusion method. Future studies are needed to determine whether the injectable ^{15}O-O_2 system can be used in other heart regions.

With the injection method, the ratio of noise equivalent counts (NEC) to total counts tended to be the higher, probably because of the absence of high radioactivity adjacent to the PET scanner. Nevertheless, the continuous-infusion method did not show this tendency. This may be because tubes for the input to the artificial lung were positioned at the femoral shunt and the output to the drain of O-15 gas was positioned alongside the PET scanner, resulting in an increase of random counts during the study. Also, it is notable that the value with the continuous-inhalation method was not small, which suggests that the inhalation protocol itself did not worsen the results, but rather the high radioactivity in the lung might affect the analysis. In any case, if more care is given to shielding of the radioactivity in tubes and/or for arrangement of instruments in the PET room, a higher value of NEC/total counts will be obtained with the injectable ^{15}O-O_2 system.

The declining slope delineated in the time-activity curves with the continuous-infusion method requires some explanation. Since the flow rate of O-15 gas supply to the artificial lung positioned at the femoral shunt was maintained constant during the PET scan, it is possible that a decrease of labeling efficiency of the artificial lung occurred due to the deposition of any components of blood. The blood of rats or humans was negligibly deposited in the artificial lung during circulation at the same rate for at least 30 min in our other experiments, so that this problem may be specific for pigs. It is unclear which component in pig blood was exactly involved in the deposition and three of four pigs did not show a declining slope of the time-activity curve.

In practice, in routine studies on myocardial oxygen metabolism using large animals such as pigs, the continuous-inhalation method with ^{15}O-O_2 gas may be easier to perform for the following reasons: (1) the intubation tube used for gas anesthesia prior to the PET scan can also be used for ^{15}O-O_2 gas inhalation; (2) catheterization of the femoral artery and vein to create the femoral shunt for the continuous-infusion method may be troublesome; and (3) the injection of ^{15}O-O_2 requires an artificial lung, preparation time, and blood taken from the same animal prior to the PET scan. However, the injection of ^{15}O-O_2 has a substantial advantage over the continuous-inhalation method in that there is reduced radioactivity in the lung and clearer images of the heart are obtained. Therefore, the method for estimating myocardial oxygen metabolism should be selected depending on the objectives of the study and the surgical procedures. Furthermore, since radioactivity administered into the femoral vein is partially excreted into expired air, the injectable ^{15}O-O_2 system might be used for evaluating pulmonary function in the future.

Conclusion

In this study, we tested the feasibility of using an injectable ^{15}O-O_2 system to estimate myocardial oxygen metabolism in pigs. Both the bolus-injection and continuous-infusion methods reduced the radioactivity in the lung and provided similar OEF values in the lateral walls of the heart. These findings indicate that the injectable ^{15}O-O_2 system has the potential to evaluate myocardial oxygen metabolism.

References

1. Ohtake T. The review of myocardial positron emission computed tomography and positron imaging by gamma camera. Kaku Igaku. 1998;35:179–87.
2. Klein LJ, Visser FC, Knaapen P, Peters JH, Teule GJ, Visser CA, et al. Carbon-11 acetate as a tracer of myocardial oxygen consumption. Eur J Nucl Med. 2001;28:651–68.
3. Schelbert HR. PET contributions to understanding normal and abnormal cardiac perfusion and metabolism. Ann Biomed Eng. 2000;28:922–9.
4. Visser FC. Imaging of cardiac metabolism using radiolabelled glucose, fatty acids and acetate. Coron Artery Dis. 2001;12(Suppl 1):S12–8.
5. Hata T, Nohara R, Fujita M, Hosokawa R, Lee L, Kudo T, et al. Noninvasive assessment of myocardial viability by positron emission tomography with ^{11}C acetate in patients with old myocardial infarction. Usefulness of low-dose dobutamine infusion. Circulation. 1996;94:1834–41.
6. Yamamoto Y, de Silva R, Rhodes CG, Iida H, Lammertsma AA, Jones T, et al. Noninvasive quantification of regional myocardial metabolic rate of oxygen by $^{15}O_2$ inhalation and positron emission tomography. Experimental validation. Circulation. 1996;94:808–16.
7. Iida H, Rhodes CG, Araujo LI, Yamamoto Y, de Silva R, Maseri A, et al. Noninvasive quantification of regional myocardial metabolic rate for oxygen by use of $^{15}O_2$ inhalation and positron emission tomography. Theory, error analysis, and application in humans. Circulation. 1996;94:792–807.
8. Shidahara M, Watabe H, Kim KM, Oka H, Sago M, Hayashi T, et al. Evaluation of a commercial PET tomograph-based system for the quantitative assessment of rCBF, rOEF and $rCMRO_2$ by using sequential administration of ^{15}O-labeled compounds. Ann Nucl Med. 2002;16:317–27.
9. Mintun MA, Raichle ME, Martin WR, Herscovitch P. Brain oxygen utilization measured with O-15 radiotracers and positron emission tomography. J Nucl Med. 1984;25:177–87.
10. Magata Y, Temma T, Iida H, Ogawa M, Mukai T, Iida Y, et al. Development of injectable O-15 oxygen and estimation of rat OEF. J Cereb Blood Flow Metab. 2003;23:671–6.
11. Temma T, Magata Y, Kuge Y, Shimonaka S, Sano K, Katada Y, et al. Estimation of oxygen metabolism in a rat model of permanent ischemia using positron emission tomography with injectable ^{15}O-O_2. J Cereb Blood Flow Metab. 2006;26:1577–83.
12. Temma T, Kuge Y, Sano K, Kamihashi J, Obokata N, Kawashima H, et al. PET O-15 cerebral blood flow and metabolism after acute stroke in spontaneously hypertensive rats. Brain Res. 2008;1212:18–24.
13. Watabe H, Jino H, Kawachi N, Teramoto N, Hayashi T, Ohta Y, et al. Parametric imaging of myocardial blood flow with ^{15}O-water and PET using the basis function method. J Nucl Med. 2005;46:1219–24.
14. Iida H, Rhodes CG, de Silva R, Yamamoto Y, Araujo LI, Maseri A, et al. Myocardial tissue fraction–correction for partial volume effects and measure of tissue viability. J Nucl Med. 1991;32:2169–75.
15. Wienhard K, Dahlbom M, Eriksson L, Michel C, Bruckbauer T, Pietrzyk U, et al. The ECAT EXACT HR: performance of a new high resolution positron scanner. J Comput Assist Tomogr. 1994;18:110–8.
16. Kudomi N, Hayashi T, Teramoto N, Watabe H, Kawachi N, Ohta Y, et al. Rapid quantitative measurement of $CMRO_2$ and CBF by dual administration of ^{15}O-labeled oxygen and water during a single PET scan-a validation study and error analysis in anesthetized monkeys. J Cereb Blood Flow Metab. 2005;25:1209–24.
17. Alders DJ, Groeneveld AB, de Kanter FJ, van Beek JH. Myocardial O_2 consumption in porcine left ventricle is heterogeneously distributed in parallel to heterogeneous O_2 delivery. Am J Physiol Heart Circ Physiol. 2004;287:H1353–61.
18. Van Woerkens EC, Trouwborst A, Duncker DJ, Koning MM, Boomsma F, Verdouw PD. Catecholamines and regional hemodynamics during isovolemic hemodilution in anesthetized pigs. J Appl Physiol. 1992;72:760–9.
19. Temma T, Magata Y, Iida H, Hayashi T, Ogawa M, Mukai T, et al. Development of injectable O-15 oxygen and its application for estimation of OEF. International Congress Series, Quantitation in Biomedical Imaging with PET and MRI Proceedings of the International Workshop on Quantitation in Biomedical Imaging with PET and MRI. 2004;1265:262–65.

Ann Nucl Med (2009) 23:843–848
DOI 10.1007/s12149-009-0319-4

ORIGINAL ARTICLE

Preparation and evaluation of $^{186/188}$Re-labeled antibody (A7) for radioimmunotherapy with rhenium(I) tricarbonyl core as a chelate site

Kazuma Ogawa · Hidekazu Kawashima · Seigo Kinuya · Kazuhiro Shiba · Masahisa Onoguchi · Hiroyuki Kimura · Kazuyuki Hashimoto · Akira Odani · Hideo Saji

Received: 16 June 2009 / Accepted: 9 September 2009 / Published online: 17 November 2009

Abstract
Objective Rhenium is one of the most valuable elements for internal radiotherapy because ^{186}Re and ^{188}Re have favorable physical characteristics. However, there are problems when proteins such as antibodies are used as carriers of $^{186/188}$Re. Labeling methods that use bifunctional chelating agents such as MAG3 require the conjugation of the $^{186/188}$Re complex to protein after radiolabeling with the bifunctional chelating agent. These processes are complicated. Therefore, we planned the preparation by a simple method and evaluation of a stable $^{186/188}$Re-labeled antibody. For this purpose, we selected $^{186/188}$Re(I) tricarbonyl complex as a chelating site. In this study, A7 (an IgG1 murine monoclonal antibody) was used as a model protein. $^{186/188}$Re-labeled A7 was prepared by directly reacting a $^{186/188}$Re(I) tricarbonyl precursor, $[^{186/188}Re(CO)_3(H_2O)_3]^+$, with A7. We then compared the biodistribution of $^{186/188}$Re-labeled A7 in tumor-bearing mice with ^{125}I-labeled A7.
Methods For labeling A7, $[^{186/188}Re(CO)_3(H_2O)_3]^+$ was prepared according to a published procedure. $^{186/188}$Re-labeled A7 ($^{186/188}$Re-$(CO)_3$-A7) was prepared by reacting $[^{186/188}Re(CO)_3(H_2O)_3]^+$ with A7 at 43°C for 2 h. Biodistribution experiments were performed by the intravenous administration of $^{186/188}$Re-$(CO)_3$-A7 solution into tumor-bearing mice.
Results ^{186}Re-$(CO)_3$-A7 and ^{188}Re-$(CO)_3$-A7 were prepared with radiochemical yields of 23 and 28%, respectively. After purification with a PD-10 column, $^{186/188}$Re-$(CO)_3$-A7 showed a radiochemical purity of over 95%. In biodistribution experiments, 13.1 and 13.2% of the injected dose/g of ^{186}Re-$(CO)_3$-A7 and ^{188}Re-$(CO)_3$-A7, respectively, accumulated in the tumor at 24-h postinjection, and the tumor-to-blood ratios were over 2.0 at the same time point. Meanwhile, uptake of ^{125}I-A7 in the tumor was almost the same as that of $^{186/188}$Re-$(CO)_3$-A7 at 24-h postinjection. Blood clearances of $^{186/188}$Re-$(CO)_3$-A7 were faster than those of ^{125}I-A7.
Conclusion $^{186/188}$Re-labeled A7 showed high uptakes in the tumor. However, further modification of the labeling method would be necessary to improve radiochemical yields and their biodistribution.

Keywords Rhenium · Radioimmunotherapy · Antibody · Tricarbonyl

K. Ogawa (✉) · A. Odani
Graduate School of Natural Science and Technology, Kanazawa University, Kakuma-machi, Kanazawa 920-1192, Japan
e-mail: kogawa@p.kanazawa-u.ac.jp

K. Ogawa · K. Shiba
Advanced Science Research Center, Kanazawa University, Kanazawa, Japan

H. Kawashima
Kyoto University Hospital, Kyoto, Japan

S. Kinuya · M. Onoguchi
Graduate School of Medical Sciences, Kanazawa University, Kanazawa, Japan

H. Kimura · H. Saji
Graduate School of Pharmaceutical Sciences, Kyoto University, Kyoto, Japan

K. Hashimoto
Japan Atomic Energy Agency, Tokai-mura, Ibaraki, Japan

Introduction

Radioimmunotherapy with radiolabeled monoclonal antibodies (mAb) has great potential to be a good treatment

modality for cancer. In particular, radioimmunotherapy in B-cell non-Hodgkin's lymphoma targeting the CD20 antigen, which is found on the B-cell surface, has clearly demonstrated its efficacy [1, 2]. Consequently, ^{90}Y ibritumomab tiuxetan (Zevalin) and ^{131}I tositumomab (Bexxar), both targeting the CD20 antigen, have been approved by the United States Food and Drug Administration for the treatment of refractory or relapsed low-grade, follicular, or transformed B-cell non-Hodgkin's lymphoma [3, 4]. Both radiopharmaceuticals have been shown to produce high response rates, but they also have some shortcomings as radionuclides. ^{131}I emits a high-energy gamma ray, 364 keV, that is not ideal for imaging and exposes patients to unnecessary radiation. Meanwhile, because ^{90}Y is a pure beta emitter, imaging is difficult with ^{90}Y-mAb, and dosimetry should be performed with ^{111}In-mAb before the ^{90}Y-mAb therapy. However, ^{111}In-mAb might not accurately predict the dosimetry of ^{90}Y-mAb because it has been reported that ^{111}In-mAb does not parallel the uptake of ^{86}Y-mAb in bone [5].

Rhenium has two useful radionuclides for radionuclide therapy, ^{186}Re and ^{188}Re. ^{186}Re and ^{188}Re are currently considered to be appropriate candidates for therapeutic applications due to their favorable nuclear properties [6, 7]. Both rhenium radioisotopes decay with the emission of not only beta particles for therapy but also gamma rays, which are suitable for external detection with gamma cameras: ^{186}Re ($t_{1/2}$ = 3.68 days, β^-_{max} = 1.07 MeV, γ = 137 keV) and ^{188}Re ($t_{1/2}$ = 16.98 h, β^-_{max} = 2.12 MeV, γ = 155 keV). In addition, in the case of ^{188}Re, a further advantage in clinical use is that ^{188}Re is conveniently produced from a transportable, in-house alumina-based ^{188}W/^{188}Re generator, similar to a ^{99}Mo/^{99m}Tc generator [8, 9].

Previous reports have demonstrated the usefulness of $^{186/188}$Re radionuclide therapy. However, there are problems when proteins such as antibodies are used as carriers of $^{186/188}$Re. A direct label method is not ideal because of the instability of labeled mAb, especially in the case of ^{186}Re [10]. The mercaptoacetylglycylglycylglycine (MAG3) ligand forms a stable ^{186}Re–MAG3 complex [11]; the usefulness of ^{186}Re–MAG3–mAb has been demonstrated in preclinical studies [12, 13]. However, the labeling method using bifunctional chelating agents such as the N_3S (MAG3) and N_2S_2 (MAMA) ligand requires conjugation with the $^{186/188}$Re complex to mAb after radiolabeling because this radiolabeling procedure requires severe conditions, such as heating and a non-neutral pH [14, 15]. These complicated processes limit the clinical utility of radiolabeled mAb. Thus, we planned the preparation by a simple method and evaluation of a stable $^{186/188}$Re-labeled protein. For this purpose, we selected $^{186/188}$Re(I) tricarbonyl complex as a chelating site. In this study, A7 (an IgG1 murine mAb) was used as a model protein, and $^{186/188}$Re-labeled A7 was prepared by directly reacting a $^{186/188}$Re(I) tricarbonyl precursor, $[^{186/188}Re(CO)_3(H_2O)_3]^+$, with A7. Then, in vitro stability experiments and biodistribution experiments in tumor-bearing mice were performed.

Materials and methods

Materials

^{186}Re and ^{188}W were supplied by the Japan Atomic Energy Agency (Tokai-mura, Japan) as $^{186}ReO_4^-$ and $^{188}WO_4^{2-}$ [16]. Alumina acid grade (100–200 mesh) alumina (ICN, Irvine, CA) was used as an adsorbent for the ^{188}W/^{188}Re generator. Silver cation exchange cartridges (Ag Plus) and anion exchange cartridges (SepPak QMA Light) were purchased from Alltech Associates, Inc. (Deerfield, IL) and Waters Corporation (Milford, MA), respectively. $^{188}ReO_4^-$ was eluted from a ^{188}W/^{188}Re generator using saline. The radioactive elution (5 mL) was condensed to a total of 400 μL using the method reported previously [8, 9]. A7, an immunoglobulin G1 murine mAb that recognizes the 45-kDa glycoprotein in human colon cancer, was used. A7 reacts with most colorectal cancers [17]. IsoLink kits for preparing $[^{186/188}Re(CO)_3(H_2O)_3]^+$ were obtained from Mallinckrodt (St Louis, MO). [^{125}I]Sodium iodide was purchased from PerkinElmer (Waltham, MA). Radiolabeling of A7 with ^{125}I was performed by the chloramine-T method [18]. Other reagents were of reagent grade and used as received.

The radiochemical purities of $^{186/188}$Re- and ^{125}I-labeled A7 were determined by thin layer chromatography (TLC) and cellulose acetate electrophoresis (CAE) (Separax-SP; Joko Co. Ltd., Tokyo, Japan). TLC analyses were performed with silica plates (Art 5553, Merck, Darmstadt, Germany) with a mixture of 99% methanol and 1% concentrated HCl as a developing solvent. CAE was run at an electrostatic field of 1.0 mA/cm for 20 min in veronal buffer (I = 0.06, pH 8.6).

Preparation of $^{186/188}$Re-labeled A7 ($^{186/188}$Re-$(CO)_3$-A7)

An intermediate of $^{186/188}$Re-labeled mAb, $[^{186/188}Re(CO)_3(H_2O)_3]^+$, was prepared using an IsoLink kit according to the method reported previously [19, 20]. Namely, a mixture of 400 μL $^{186/188}ReO_4^-$ and 6 μL concentrated phosphoric acid was added to an IsoLink kit to which 6 mg $BH_3{\cdot}NH_3$ (Aldrich, Milwaukee, WI) had previously been added. The reaction mixture was heated at 65°C for 15 min with a 20 mL syringe inserted to balance the pressure caused by gas production during the reaction. After the $^{186/188}$Re tricarbonyl intermediate solution was adjusted to about pH 7, 200 μL of this solution was added to 80 μL of the A7 mAb

solution (14.7 mg/mL). After 2 h of incubation at 43°C, this reaction mixture was purified with a PD-10 column (GE Healthcare UK Ltd., Buckinghamshire, England) with saline as the eluate.

In vitro stability

To evaluate its stability, ^{188}Re-$(CO)_3$-A7 in saline solution was incubated at 37°C. After incubation for 24 h, a sample was drawn and its radioactivity was analyzed by CAE and TLC. In addition, ^{188}Re-$(CO)_3$-A7 solutions were diluted 10-fold with a 0.1 M solution of histidine or freshly prepared murine plasma, and the solutions were incubated at 37°C. After 1-, 3-, and 24-h incubation, the radioactivity of each sample was analyzed by TLC.

Biodistribution in tumor-bearing mice

Experiments with animals were conducted in accordance with the Guidelines for the Care and Use of Laboratory Animals of Kanazawa University. The animals were housed with free access to food and water at 23°C with a 12-h alternating light/dark schedule. LS180 human colon carcinoma cells were obtained from ATCC (Manassas, VA) and grown in cell culture dishes in Eagle's minimum essential medium with phenol red, 10% heat-inactivated fetal calf serum, 100 μg/mL glutamine, 100 units/mL penicillin, and 100 μg/mL streptomycin. The cells were cultured in a humidified atmosphere of 95% air and 5% carbon dioxide at 37°C. They were then released from the dishes by treatment with 0.05% trypsin/EDTA. Next, to produce tumors, the mice to be inoculated were anesthetized with pentobarbital and approximately 5×10^6 cells were injected subcutaneously into the right shoulder of 4-week-old BALB/c nu/nu female mice (15–19 g). Biodistribution experiments were performed approximately 8 days postinoculation, i.e., the time required for the tumors to reach a palpable size. Groups of four or five mice were administered 100 μL ^{186}Re-$(CO)_3$-A7, ^{188}Re-$(CO)_3$-A7, or ^{125}I-A7 (7.4 kBq, A7: 100 μg, respectively) intravenously and killed at 1- and 24-h postinjection. Tissues of interest were removed and weighed, and radioactivity counts were determined with an Auto Well Gamma System (ARC-380; Aloka, Tokyo, Japan) and corrected for background radiation and physical decay during counting.

Results

Preparation of $^{186/188}$Re-$(CO)_3$-A7

In TLC analyses, $^{186/188}$Re-$(CO)_3$-A7 remained at the original position (Rf = 0), while an intermediate, $[^{186/188}Re(CO)_3(H_2O)_3]^+$, and the free perrhenate ($^{186/188}ReO_4^-$) migrated to Rf = 0.2–0.4 and Rf = 0.7–0.8, respectively [20]. In CAE analyses, intact A7 migrated to the 2–2.5 cm anode from the origin, which was determined by Ponceau S dye, and $^{186/188}$Re-$(CO)_3$-A7 also migrated to the 2–2.5 cm anode (Fig. 1), while colloidal $^{186/188}$Re remained at the origin. The radiolabeling yield of $[^{188}Re(CO)_3(H_2O)_3]^+$ was 41%. ^{186}Re-$(CO)_3$-A7 and ^{188}Re-$(CO)_3$-A7 were prepared with radiochemical yields of 23 and 28%, respectively. After purification using a PD-10 column, ^{186}Re-$(CO)_3$-A7 and ^{188}Re-$(CO)_3$-A7 showed a radiochemical purity of over 95%.

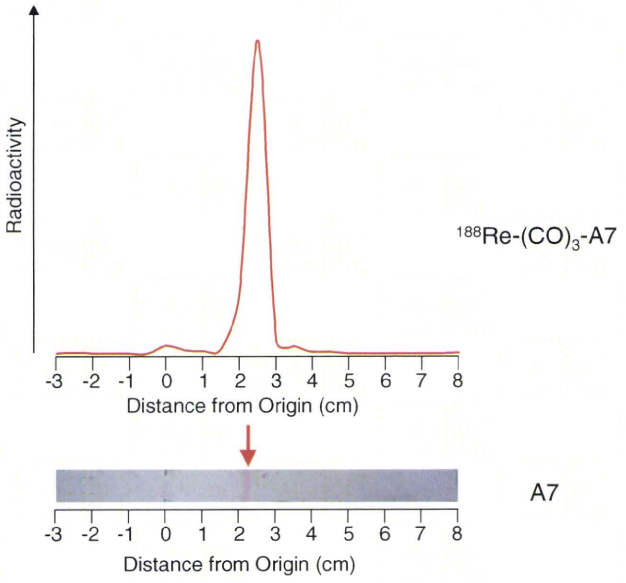

Fig. 1 Profiles of ^{188}Re-$(CO)_3$-A7 and intact A7 (Ponceau S dye) on cellulose acetate electrophoresis

In vitro stability

After incubation in saline for 24 h, about 93% of the ^{188}Re-$(CO)_3$-A7 remained intact. In murine plasma, over 90% of radioactivity existed in a protein fraction for 24 h, indicating that the ^{188}Re-$(CO)_3$-A7 is not degraded to $^{188}ReO_4^-$ in plasma. When challenged with an excess of histidine, part of the radioactivity dissociated from ^{188}Re-$(CO)_3$-A7 (Fig. 2).

Biodistribution in tumor-bearing mice

The biodistributions of ^{186}Re-$(CO)_3$-A7, ^{188}Re-$(CO)_3$-A7, and ^{125}I-A7 in tumor-bearing mice are listed in Tables 1, 2, and 3. As we expected, both radiorhenium-labeled A7 had almost identical biodistribution. ^{186}Re-$(CO)_3$-A7 and ^{188}Re-$(CO)_3$-A7 showed high uptakes in the tumors, amounting to 13.1 and 13.2% at 24-h postinjection, respectively. Meanwhile, uptake of ^{125}I-A7 in the tumor

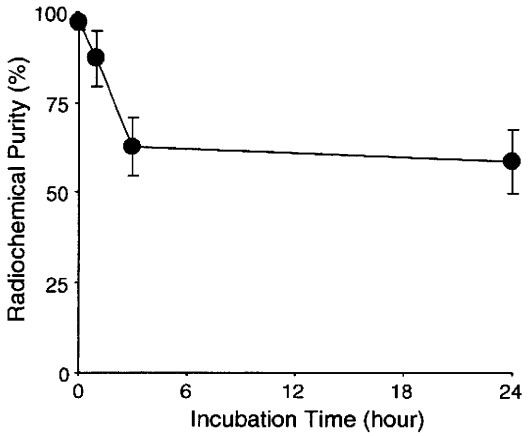

Fig. 2 Stability of ^{188}Re-$(CO)_3$-A7 in L-histidine solution

Table 1 Biodistribution of radioactivity after intravenous administration of ^{186}Re-$(CO)_3$-A7 in mice

Tissue	Time after administration	
	1 h	24 h
Blood	24.8 (1.1)	6.2 (0.3)
Tumor	5.1 (0.7)	13.1 (1.8)
Liver	18.5 (0.4)	9.7 (0.8)
Kidney	13.8 (0.4)	9.0 (1.1)
Intestine	1.5 (0.3)	2.0 (0.2)
Spleen	7.8 (1.0)	4.5 (0.9)
Pancreas	1.1 (0.1)	0.9 (0.0)
Lung	11.8 (2.5)	3.8 (0.5)
Heart	4.4 (0.6)	1.8 (0.1)
Stomach[a]	0.4 (0.0)	0.2 (0.0)
Muscle	0.9 (0.4)	0.8 (0.1)

Data are expressed as % injected dose per gram tissue. Each value represents the mean (SD) of four or five animals

[a] Data are expressed as % injected dose

was almost the same as that of $^{186/188}$Re-$(CO)_3$-A7 at 24-h postinjection. Blood clearances of $^{186/188}$Re-$(CO)_3$-A7 were faster than that of ^{125}I-A7. $^{186/188}$Re-$(CO)_3$-A7 showed that the tumor/blood ratios were over 2.0 at 24-h postinjection, but the tumor/blood ratio of ^{125}I-A7 was approximately 1.0.

Discussion

We hypothesize that the $^{186/188}$Re$(CO)_3$ core binds endogenous histidine residue in an antibody when $[^{186/188}Re(CO)_3(H_2O)_3]^+$ is used to label the antibody. In our preliminary experiments, we labeled H-His-OMe with $[^{186}Re(CO)_3(H_2O)_3]^+$ at room temperature, 45°C, or 100°C. As a result, the radiochemical yield increased in a

Table 2 Biodistribution of radioactivity after intravenous administration of ^{188}Re-$(CO)_3$-A7 in mice

Tissue	Time after administration	
	1 h	24 h
Blood	27.6 (1.8)	5.9 (0.8)
Tumor	6.0 (1.7)	13.2 (1.7)
Liver	18.9 (2.8)	9.7 (0.8)
Kidney	14.8 (1.7)	8.9 (0.4)
Intestine	1.8 (0.2)	2.0 (0.3)
Spleen	8.3 (0.8)	4.0 (0.7)
Pancreas	1.5 (0.2)	0.8 (0.0)
Lung	12.6 (2.2)	3.2 (0.4)
Heart	5.6 (0.5)	1.6 (0.3)
Stomach[a]	0.9 (0.2)	0.3 (0.1)
Muscle	0.8 (0.2)	0.5 (0.1)

Data are expressed as % injected dose per gram tissue. Each value represents the mean (SD) of four or five animals

[a] Data are expressed as % injected dose

Table 3 Biodistribution of radioactivity after intravenous administration of ^{125}I-A7 in mice

Tissue	Time after administration	
	1 h	24 h
Blood	36.7 (4.3)	13.6 (2.1)
Tumor	3.5 (0.7)	13.9 (3.5)
Liver	10.7 (4.5)	3.4 (1.0)
Kidney	8.3 (1.4)	2.9 (0.7)
Intestine	1.6 (0.3)	1.0 (0.3)
Spleen	7.5 (3.2)	2.5 (0.8)
Pancreas	1.3 (0.4)	1.2 (0.2)
Lung	19.8 (2.5)	7.8 (1.2)
Heart	6.9 (1.0)	3.1 (0.5)
Stomach[a]	1.2 (0.2)	1.0 (0.4)
Muscle	0.9 (0.2)	0.8 (0.1)

Data are expressed as % injected dose per gram tissue. Each value represents the mean (SD) of four animals

[a] Data are expressed as % injected dose

reaction temperature-dependent manner. In this study, A7 was reacted with $[^{186/188}Re(CO)_3(H_2O)_3]^+$ at 43°C because higher temperatures damage the antibody. Radiochemical yields of $^{186/188}$Re-labeled A7 were less than 30%. For clinical use, the radiochemical purity should be over 95% without purification. We suppose that some sequences, such as an oligohistidine sequence, could be inserted into the antibody to improve the radiochemical yield. Tait et al. [21] reported that $(His)_6$-inserted annexin V had a better radiochemical yield compared with those of $(His)_3$-inserted annexin V and wild-type annexin V when annexin V was

labeled with $[^{99m}Tc(CO)_3(H_2O)_3]^+$. Another cause of low radiochemical yields of $^{186/188}$Re-labeled A7 could be low yields of $[^{186/188}Re(CO)_3(H_2O)_3]^+$. In this study, the radiochemical yield of $[^{188}Re(CO)_3(H_2O)_3]^+$ was only 41%. Recently, higher yields of the preparation of the precursor, $[^{188}Re(CO)_3(H_2O)_3]^+$, were reported [22, 23]. We assume that using the new method for preparing $[^{186/188}Re(CO)_3(H_2O)_3]^+$ in future studies would also improve the radiochemical yields of $^{186/188}$Re-labeled A7.

The high stability of ^{188}Re-$(CO)_3$-A7 in saline and almost no degradation to $^{188}ReO_4^-$ in plasma were shown in in vitro experiments. Since accumulation in the stomach is an index of ReO_4^- in biodistribution studies [24], low radioactivity levels in the stomach after injection of $^{186/188}$Re-$(CO)_3$-A7 indicate little decomposition to $^{186/188}ReO_4^-$ in vivo. In a recent study, Chen et al. [23] prepared a ^{188}Re-labeled antibody (^{188}Re(I)-trastuzumab) by a similar method. ^{188}Re(I)-trastuzumab showed high stability in vitro and low stomach accumulation in tumor-bearing mice. These studies strongly support the validity of our results.

In other previous studies, it was reported that a radioiodine-labeled antibody, ^{88}Y-isothiocyanatobenzyl-DTPA-antibody, and ^{186}Re-MAG3-antibody showed similar blood clearances [25, 26]. However, in this study, the radioactivity (%dose/g) in blood at 24-h postinjection of ^{186}Re-$(CO)_3$-A7, ^{188}Re-$(CO)_3$-A7, and ^{125}I-A7 was 6.2 ± 0.3, 5.9 ± 0.8, and 13.9 ± 3.5, respectively. That is, $^{186/188}$Re-$(CO)_3$-A7 showed faster blood clearance compared with that of ^{125}I-A7 in the biodistribution experiments. These results suggest that $^{186/188}$Re detached from A7 in the blood flow. There is a possibility that the binding of the $^{186/188}$Re-$(CO)_3$ core to A7 is not strong, and so some molecules in the blood might remove the $^{186/188}$Re-$(CO)_3$ core from $^{186/188}$Re-$(CO)_3$-A7. Actually, when ^{188}Re-$(CO)_3$-A7 was challenged with an excess of histidine, part of the radioactivity dissociated from ^{188}Re-$(CO)_3$-A7. In this experiment, the radiochemical purity of ^{188}Re-$(CO)_3$-A7 decreased to around 60% after 3-h incubation. However, after 24-h incubation, the radiochemical purity of ^{188}Re-$(CO)_3$-A7 was almost same as that after 3-h incubation. These results suggest that there are strong and weak bindings of the ^{188}Re-$(CO)_3$ core to an A7 antibody in purified ^{188}Re-$(CO)_3$-A7 because the ^{188}Re-$(CO)_3$ core does not bind to a specific site in an antibody. Recently, the biodistribution of $[^{188}Re(CO)_3(H_2O)_3]^+$ was reported [27]. The radioactivity in blood, liver, and kidney at 24-h postinjection of $[^{188}Re(CO)_3(H_2O)_3]^+$ were 3.13 ± 0.52, 9.65 ± 1.40, and 9.62 ± 0.09, respectively. Taking into account the biodistribution at 24-h postinjection of $^{186/188}$Re-$(CO)_3$-A7 in this study, these results are also not inconsistent with our hypothesis.

Faster blood clearance is advantageous for mitigating side effects because myelosuppression is the chief side effect associated with radioimmunotherapy [28]. However, faster blood clearance compromises the accumulation of radioactivity in tumors. In summary, although diagnostic radiopharmaceuticals should be better because they need a high tumor/blood ratio at an earlier time postinjection, therapeutic radiopharmaceuticals might be unfavorable because high accumulation and long retention in tumors are preferred for a better therapeutic effect. As mentioned above, we suppose that insertion of an oligohistidine sequence could improve the radiochemical yield. In addition, insertion could also be effective from the point of view of improving the in vivo stability and biodistribution of $^{186/188}$Re-labeled antibodies.

Conclusion

$^{186/188}$Re-labeled A7 showed high uptakes in tumors the same as that of ^{125}I-labeled A7. However, further modifications of the labeling method would be necessary in order to improve radiochemical yields and their biodistribution.

References

1. Macklis RM. Radioimmunotherapy as a therapeutic option for non-Hodgkin's lymphoma. Semin Radiat Oncol. 2007;17:176–83.
2. Dillman RO. Radioimmunotherapy of B-cell lymphoma with radiolabelled anti-CD20 monoclonal antibodies. Clin Exp Med. 2006;6:1–12.
3. Davies AJ. Radioimmunotherapy for B-cell lymphoma: Y^{90} ibritumomab tiuxetan and I^{131} tositumomab. Oncogene. 2007;26:3614–28.
4. Jacene HA, Filice R, Kasecamp W, Wahl RL. Comparison of ^{90}Y-ibritumomab tiuxetan and ^{131}I-tositumomab in clinical practice. J Nucl Med. 2007;48:1767–76.
5. Garmestani K, Milenic DE, Plascjak PS, Brechbiel MW. A new and convenient method for purification of ^{86}Y using a Sr(II) selective resin and comparison of biodistribution of ^{86}Y and ^{111}In labeled Herceptin. Nucl Med Biol. 2002;29:599–606.
6. Ogawa K, Mukai T, Asano D, Kawashima H, Kinuya S, Shiba K, et al. Therapeutic effects of a ^{186}Re-complex-conjugated bisphosphonate for the palliation of metastatic bone pain in an animal model. J Nucl Med. 2007;48:122–7.
7. Ferro-Flores G, Arteaga de Murphy C. Pharmacokinetics and dosimetry of ^{188}Re-pharmaceuticals. Adv Drug Deliv Rev. 2008;60:1389–401.
8. Knapp FF Jr, Beets AL, Guhlke S, Zamora PO, Bender H, Palmedo H, et al. Availability of rhenium-188 from the alumina-based tungsten-188/rhenium-188 generator for preparation of rhenium-188-labeled radiopharmaceuticals for cancer treatment. Anticancer Res. 1997;17:1783–95.
9. Guhlke S, Beets AL, Oetjen K, Mirzadeh S, Biersack HJ, Knapp FF Jr. Simple new method for effective concentration of ^{188}Re solutions from alumina-based ^{188}W–^{188}Re generator. J Nucl Med. 2000;41:1271–8.
10. Griffiths GL, Goldenberg DM, Knapp FF Jr, Callahan AP, Chang CH, Hansen HJ. Direct radiolabeling of monoclonal antibodies

with generator-produced rhenium-188 for radioimmunotherapy: labeling and animal biodistribution studies. Cancer Res. 1991;51:4594–602.
11. Ogawa K, Mukai T, Arano Y, Ono M, Hanaoka H, Ishino S, et al. Development of a rhenium-186-labeled MAG3-conjugated bisphosphonate for the palliation of metastatic bone pain based on the concept of bifunctional radiopharmaceuticals. Bioconjug Chem. 2005;16:751–7.
12. Kinuya S, Yokoyama K, Tega H, Hiramatsu T, Konishi S, Yamamoto W, et al. Rhenium-186-mercaptoacetyltriglycine-labeled monoclonal antibody for radioimmunotherapy: in vitro assessment, in vivo kinetics and dosimetry in tumor-bearing nude mice. Jpn J Cancer Res. 1998;89:870–8.
13. Kinuya S, Yokoyama K, Kobayashi K, Motoishi S, Onoma K, Watanabe N, et al. Experimental radioimmunotherapy with ^{186}Re–MAG3–A7 anti-colorectal cancer monoclonal antibody: comparison with ^{131}I-counterpart. Ann Nucl Med. 2001;15:199–202.
14. Visser GW, Gerretsen M, Herscheid JD, Snow GB, van Dongen G. Labeling of monoclonal antibodies with rhenium-186 using the MAG3 chelate for radioimmunotherapy of cancer: a technical protocol. J Nucl Med. 1993;34:1953–63.
15. Ogawa K, Mukai T, Arano Y, Otaka A, Ueda M, Uehara T, et al. Rhenium-186-monoaminemonoamidedithiol-conjugated bisphosphonate derivatives for bone pain palliation. Nucl Med Biol. 2006;33:513–20.
16. Kobayashi K, Motoishi S, Terunuma K, Rauf AA, Hashimoto K. Production of ^{186,188}Re and recovery of tungsten from spent ^{188}W/^{188}Re generator. Radiochemistry. 2000;42:551–4.
17. Kotanagi H, Takahashi T, Masuko T, Hashimoto Y, Koyama K. A monoclonal antibody against human colon cancers. Tohoku J Exp Med. 1986;148:353–60.
18. Wilbur DS, Hadley SW, Grant LM, Hylarides MD. Radioiodinated iodobenzoyl conjugates of a monoclonal antibody Fab fragment. In vivo comparisons with chloramine-T-labeled Fab. Bioconjug Chem. 1991;2:111–6.
19. He J, Liu C, Vanderheyden JL, Liu G, Dou S, Rusckowski M, et al. Radiolabelling morpholinos with ^{188}Re tricarbonyl provides improved in vitro and in vivo stability to re-oxidation. Nucl Med Commun. 2004;25:731–6.
20. Schibli R, Schwarzbach R, Alberto R, Ortner K, Schmalle H, Dumas C, et al. Steps toward high specific activity labeling of biomolecules for therapeutic application: preparation of precursor $[^{188}Re(H_2O)_3(CO)_3]^+$ and synthesis of tailor-made bifunctional ligand systems. Bioconjug Chem. 2002;13:750–6.
21. Tait JF, Smith C, Gibson DF. Development of annexin V mutants suitable for labeling with Tc(i)-carbonyl complex. Bioconjug Chem. 2002;13:1119–23.
22. Park SH, Seifert S, Pietzsch HJ. Novel and efficient preparation of precursor $[^{188}Re(OH_2)_3(CO)_3]^+$ for the labeling of biomolecules. Bioconjug Chem. 2006;17:223–5.
23. Chen KT, Lee TW, Lo JM. In vivo examination of ^{188}Re(I)-tricarbonyl-labeled trastuzumab to target HER2-overexpressing breast cancer. Nucl Med Biol. 2009;36:355–61.
24. Lin WY, Hsieh JF, Tsai SC, Yen TC, Wang SJ, Knapp FF Jr. A comprehensive study on the blockage of thyroid and gastric uptakes of ^{188}Re-perrhenate in endovascular irradiation using liquid-filled balloon to prevent restenosis. Nucl Med Biol. 2000;27:83–7.
25. Brouwers AH, van Eerd JE, Frielink C, Oosterwijk E, Oyen WJ, Corstens FH, et al. Optimization of radioimmunotherapy of renal cell carcinoma: labeling of monoclonal antibody cG250 with ^{131}I, ^{90}Y, ^{177}Lu, or ^{186}Re. J Nucl Med. 2004;45:327–37.
26. Koppe MJ, Bleichrodt RP, Soede AC, Verhofstad AA, Goldenberg DM, Oyen WJ, et al. Biodistribution and therapeutic efficacy of $^{125/131}$I-, ^{186}Re-, $^{88/90}$Y-, or ^{177}Lu-labeled monoclonal antibody MN-14 to carcinoembryonic antigen in mice with small peritoneal metastases of colorectal origin. J Nucl Med. 2004;45:1224–32.
27. Xia JY, Wang YX, Li GC, Yu JF, Yin DZ. Synthesis of pyridyl derivatives for the future functionalization of biomolecules labeled with the fac-[Re-188$(CO)_3(H_2O)_3]^+$ precursor. J Radioanal Nucl Chem. 2009;279:245–52.
28. Oriuchi N, Higuchi T, Hanaoka H, Iida Y, Endo K. Current status of cancer therapy with radiolabeled monoclonal antibody. Ann Nucl Med. 2005;19:355–65.

Available online at www.sciencedirect.com
ScienceDirect
Nuclear Medicine and Biology 36 (2009) 129–135
NUCLEAR MEDICINE — AND — BIOLOGY
www.elsevier.com/locate/nucmedbio

Development of [^{90}Y]DOTA-conjugated bisphosphonate for treatment of painful bone metastases

Kazuma Ogawa[a,*], Hidekazu Kawashima[b,c], Kazuhiro Shiba[a], Kohshin Washiyama[d], Mitsuyoshi Yoshimoto[d], Yasushi Kiyono[e,f], Masashi Ueda[b,f], Hirofumi Mori[a], Hideo Saji[b]

[a]*Advanced Science Research Center, Kanazawa University, Kanazawa 920-8640, Japan*
[b]*Graduate School of Pharmaceutical Sciences, Kyoto University, Kyoto 606-8501, Japan*
[c]*Graduate School of Medicine, Kyoto University, Kyoto 606-8507, Japan*
[d]*Division of Health Sciences, Graduate School of Medical Science, Kanazawa University, Kanazawa 920-0942, Japan*
[e]*Biomedical Imaging Research Center, University of Fukui, Yoshida-gun 910-1193, Japan*
[f]*Radioisotopes Research Laboratory, Kyoto University Hospital, Faculty of Medicine, Kyoto University, Kyoto 606-8507, Japan*

Received 19 December 2007; received in revised form 23 September 2008; accepted 19 November 2008

Abstract

Introduction: Based on the concept of bifunctional radiopharmaceuticals, we have previously developed ^{186}Re-complex-conjugated bisphosphonate analogs for palliation of painful bone metastases and have demonstrated the utility of these compounds. By applying a similar concept, we hypothesized that a bone-specific directed ^{90}Y-labeled radiopharmaceutical could be developed.
Methods: In this study, 1,4,7,10-tetraazacyclododecane-1,4,7,10-tetraacetic acid (DOTA) was chosen as the chelating site, and DOTA was conjugated with 4-amino-1-hydroxybutylidene-1,1-bisphosphonate. [^{90}Y]DOTA-complex-conjugated bisphosphonate ([^{90}Y]DOTA-HBP) was prepared by coordination with ^{90}Y, and its biodistribution was studied in comparison to [^{90}Y]citrate.
Results: In biodistribution experiments, [^{90}Y]DOTA-HBP and [^{90}Y]citrate rapidly accumulated and resided in the bone. Although [^{90}Y]citrate showed a higher level of accumulation in the bone than [^{90}Y]DOTA-HBP, the clearances of [^{90}Y]DOTA-HBP from the blood and from almost all soft tissues were much faster than those of [^{90}Y]citrate. As a result, the estimated absorbed dose ratios of soft tissues to osteogenic cells (target organ) of [^{90}Y]DOTA-HBP were lower than those of [^{90}Y]citrate.
Conclusions: [^{90}Y]DOTA-HBP showed superior biodistribution characteristics as a bone-seeking agent and led to a decrease in the level of unnecessary radiation compared to [^{90}Y]citrate. Since the DOTA ligand forms a stable complex not only with ^{90}Y but also with lutetium (^{177}Lu), indium (^{111}In), gallium ($^{67/68}$Ga), gadolinium (Gd) and so on, complexes of DOTA-conjugated bisphosphonate with various metals could be useful as agents for palliation of metastatic bone pain, bone scintigraphy and magnetic resonance imaging.

Keywords: Yttrium-90; DOTA; Bisphosphonate; Bone; Palliation; Radiation dose

1. Introduction

Malignant tumors, especially in the advanced stages of prostate, breast and lung carcinomas, frequently metastasize to the bone. A prominent symptom of such metastasis is severe pain, which has a significant impact on patients' quality of life, and bone metastases are the most common cause of pain in patients with malignant disease [1–3]. Management of pain is a challenging clinical problem, but controlling bone pain is difficult, especially in the later stages of the disease.

Localized radiation therapy is an effective method for the treatment of bone pain [4]. Unfortunately, however, bone pain often recurs at treated sites, and second radiation therapy seldom provides full palliation of pain. In addition, localized radiation therapy is difficult to apply when there are multiple lesion sites, as is often the case in patients with bone metastases. In such cases, systemic radionuclide therapy using specifically localized bone-seeking radiopharmaceuticals is preferable because of few side effects, long-lived therapeutic effects by single injection and repeated usability [5].

* Corresponding author. Tel.: +81 76 265 2476; fax: +81 76 234 4245.
E-mail address: kogawa@med.kanazawa-u.ac.jp (K. Ogawa).

0969-8051/$ – see front matter © 2009 Elsevier Inc. All rights reserved.
doi:10.1016/j.nucmedbio.2008.11.007

Yttrium-90 is a pure β^--emitter (E_{max}=2.28 MeV) with a half-life of 64.1 h. The usefulness of [^{90}Y]citrate for bone pain palliation in clinical use has been reported [6]. Although [^{90}Y]citrate indicates high accumulation in the bone, some part of the Y^{3+} released by the dissociation of the citrate complex binds to serum, which results in delayed blood clearance and accumulation in the liver [7]. Meanwhile, based on the concept of bifunctional radiopharmaceuticals, we have previously developed ^{186}Re-complex-conjugated bisphosphonate analogs to improve the stability of [^{186}Re]bisphosphonate complex for palliation of painful bone metastases, and we have demonstrated the utility of these compounds [8–13]. By applying a similar concept, we hypothesized that a stable and bone-specific directed ^{90}Y-labeled radiopharmaceutical could be developed. In this study, 1,4,7,10-tetraazacyclododecane-1,4,7,10-tetraacetic acid (DOTA) was chosen as the chelating site because it forms a stable complex with ^{90}Y, and DOTA was conjugated with 4-amino-1-hydroxybutylidene-1,1-bisphosphonate. Then, [^{90}Y]DOTA-complex-conjugated bisphosphonate ([^{90}Y]DOTA-HBP) was prepared by coordination with ^{90}Y, and its biodistribution was studied in comparison to [^{90}Y]citrate.

2. Materials and methods

2.1. Materials

Electrospray ionization mass spectra were obtained with an LCMS-QP8000α (Shimadzu, Kyoto, Japan). Thin-layer chromatography analyses were performed with silica plates (Art 5553; Merck, Darmstadt, Germany), with 1.3 M ammonium acetate–methanol (1:1) as developing solvent. [^{90}Y]Yttrium chloride ($^{90}YCl_3$) in 0.04 M HCl was kindly supplied by Chiyoda Technol Corp. (Tokyo, Japan). 1,4,7,10-Tetraazacyclododecane-1,4,7,10-tetraacetic acid mono(*N*-hydroxysuccinimidyl ester) (DOTA-NHS-ester) (**1**) was purchased from Macrocyclics (Dallas, TX). Other reagents were of reagent grade and were used as received.

2.2. Synthesis of DOTA-conjugated bisphosphonate (DOTA-HBP (3))

DOTA-HBP (**3**) was synthesized by conjugation of the DOTA ligand to a bisphosphonate derivative (Scheme 1). Specifically, 4-amino-1-hydroxybutylidene-1-1-bisphosphonate (**2**) (12.4 mg, 0.05 mmol), synthesized as described previously [9], was suspended in 665 μl of distilled water, and triethylamine (30.0 mg, 0.30 mmol) was added to the suspension. After a few seconds of stirring at room temperature, the suspension became clear. DOTA-NHS-ester (**1**) (60.1 mg, 0.06 mmol) was dissolved in 665 μl of dimethylformamide and then gradually added to the reaction mixture. Triethylamine (60.0 mg, 0.59 mmol) was then added, and the reaction mixture was stirred for 24 h at room temperature. The mixture was purified by reversed-phase high-performance liquid chromatography (RP-HPLC) performed with a Hydrosphere C18 column (20×150 mm; YMC, Kyoto, Japan) at a flow rate of 12 ml/min with a mobile phase of 0.1% trifluoroacetic acid (TFA) in water. Chromatograms were obtained by monitoring UV adsorption at a wavelength of 220 nm. The fraction containing DOTA-HBP (**3**) was determined by mass spectrometry and collected. The solvent was removed by lyophilization to provide DOTA-HBP (**3**) (6.1 mg, 19.2%) as white crystals: MS (ESI) calculated for $C_{20}H_{39}N_5O_{14}P_2$ $(M-H)^-$: *m/z* 634; found: 634.

2.3. Preparation of [^{90}Y]DOTA-HBP

DOTA-HBP (**3**) (0.1 mg) was dissolved in 50 μl of 1.3 M ammonium acetate, and $^{90}YCl_3$ in 0.04 M HCl was added to the solution. The mixture was reacted at 95°C for 15 min. [^{90}Y]DOTA-HBP was purified by RP-HPLC performed with a Hydrosphere C18 column (4.6×250 mm) at a flow rate of 1 ml/min with a mobile phase of 0.1% TFA in water.

2.4. Preparation of [^{90}Y]citrate

[^{90}Y]Citrate was prepared according to the procedures described previously [7]. Briefly, $^{90}YCl_3$ in 0.04 M HCl was added to a 3-ml aqueous solution of 7.5 mg/ml sodium citrate.

2.5. Stability of [^{90}Y]DOTA-HBP in plasma

[^{90}Y]DOTA-HBP was diluted 10-fold with freshly prepared rat plasma, and the solutions were incubated at 37°C for 24 h. After 1, 3 and 24 h of incubation, 100-μl aliquots of the samples were drawn and mixed with the same volume of 0.1% TFA aqueous solution. After centrifugation at 6300×*g* for 2 min, 60 μl of supernatant was analyzed by RP-HPLC.

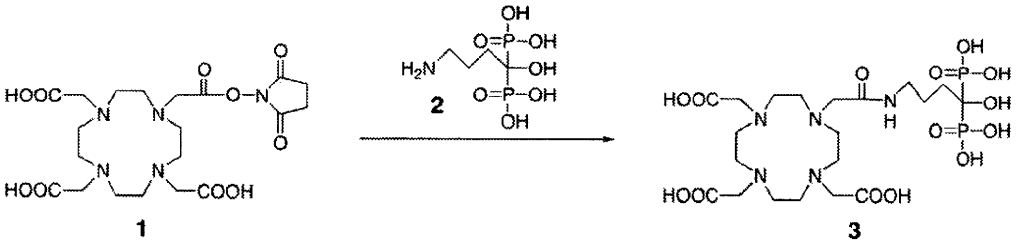

Scheme 1. Synthesis of DOTA-HBP.

2.6. Biodistribution experiments

Animal experiments were conducted in accordance with our institutional guidelines; experimental procedures were approved by the Kyoto University Animal Care Committee. Biodistribution experiments were performed with an intravenous administration of 100 μl of each diluted tracer solution to 6-week-old male ddY mice (27–30 g; Japan SLC, Inc., Hamamatsu, Japan). Groups of five mice each were sacrificed by decapitation at 10, 60 and 180 min postinjection. Tissues of interest were removed and weighed. The complete left femur was isolated as a representative bone sample. The levels of radioactivity in these tissues were determined as bremsstrahlung with an autowell gamma counter (ARC-380; Aloka, Tokyo, Japan) using a very large energy window and corrected for background radiation and physical decay during counting.

2.7. Radiation dose estimates

For estimation of the radiation dose absorbed by the bone and bone marrow, the activity concentration in the bone marrow was assumed to be 30% of the activity concentration in the blood [14]. A red marrow mass was assumed to be 25% of blood volume [14]. The blood, bone and muscle mass of mice were assumed to be 8%, 5% and 48% of body weight, respectively. According to the International Commission on Radiological Protection, an equal distribution of radionuclide to trabecular and cortical bones was assumed [15]. The non-decay-corrected activity from each source organ was converted into a percentage of the injected dose. The area under each organ's activity curve from Time 0 to infinity was calculated by extrapolation of biodistribution data. To correct for the different ratios of organ to total body weights in mouse or rat and in human, we used the following organ correction factor (CR):

$$CR = (\text{organ mass/total body mass})_{\text{human}} / (\text{organ mass/total body mass})_{\text{mouse or rat}}.$$

According to the values, the radiation doses were calculated for an adult male patient using OLINDA 1.0 software (Vanderbilt University) [16].

2.8. Statistical analysis

Biodistribution data were compared using Students' *t* test. $P=.05$ was set as the limit of significance.

3. Results

3.1. Preparation of [^{90}Y]DOTA-HBP

The labeling efficiency of DOTA with ^{90}Y should be very high [17,18]. In this study, however, the radiochemical yields of [^{90}Y]DOTA-HBP ranged from 54% to 80%. Fig. 1A is a typical radiochromatogram of [^{90}Y]DOTA-HBP before purification. Radioimpurity showed a peak at 9 min, and

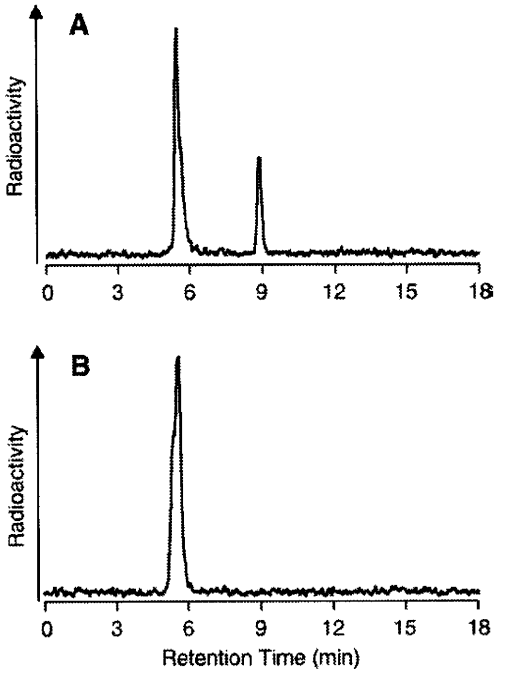

Fig. 1. RP-HPLC radiochromatograms of [^{90}Y]DOTA-HBP before purification (A) and after purification (B). Conditions: flow rate of 1 ml/min with 0.1% TFA in water.

the peak of [^{90}Y]DOTA, which was reacted between $^{90}YCl_3$ and the DOTA ligand, coincided with the peak of radioimpurity. On RP-HPLC analysis after the synthesis reaction of DOTA-HBP, the peaks of DOTA-HBP and DOTA-NHS-ester were observed to be close. When we purified DOTA-HBP by RP-HPLC, a subtle amount of DOTA-NHS-ester might have mixed with DOTA-HBP. As a result of DOTA-NHS-ester hydrolyzation to DOTA, [^{90}Y]DOTA might mix as an impurity. After purification by RP-HPLC, [^{90}Y]DOTA-HBP had a radiochemical purity of over 95% (Fig. 1B).

3.2. Stability of [^{90}Y]DOTA-HBP in plasma

Table 1 shows the stability of [^{90}Y]DOTA-HBP in plasma. Although it was nearly intact after 1 h of incubation, it gradually decomposed over time.

3.3. Biodistribution experiments

The biodistributions of [^{90}Y]DOTA-HBP and [^{90}Y]citrate in normal mice are presented in Tables 2 and 3, respectively. Both ^{90}Y-labeled compounds accumulated rapidly and resided in the bone. Although the difference in the accumulation of both compounds in the bone was not significant at 10 min postinjection, [^{90}Y]citrate accumulated in the bone in significantly larger amounts than [^{90}Y]DOTA-HBP at 60 and 180 min postinjection. However, the blood clearance of [^{90}Y]DOTA-HBP was much faster than that of [^{90}Y]citrate, and the radioactivity of [^{90}Y]DOTA-HBP was barely observed in tissues other than bone at 180 min postinjection. In addition, the clearances of [^{90}Y]citrate were slower than those of [^{90}Y]DOTA-HBP in almost all tissues.

Table 1
Stability of [^{90}Y]DOTA-HBP in plasma

Incubation period (h)	Radiochemical purity (%)
1	94.0 (0.49)
3	84.5 (0.38)
24	35.7 (3.02)

Each value represents the mean (S.D.) for three experiments.

3.4. Dosimetry

Table 4 shows the estimates of absorbed radiation doses for [^{90}Y]DOTA-HBP, [^{90}Y]citrate and [^{153}Sm]ethylene diamine tetramethylene phosphonate (EDTPM). In the case of [^{153}Sm]EDTPM, calculation was performed using the data of a biodistribution study reported previously [19]. Table 5 shows the ratios between the estimates of the absorbed doses for some organs and osteogenic cells. Since osteogenic cells are assumed to be the target for internal radionuclide therapy using bone-seeking radiopharmaceuticals, these ratios can be regarded as an index of unnecessary radiation in obtaining an equal therapeutic effect. The absorbed dose ratios of red marrow to osteogenic cells and total body to osteogenic cells were almost the same for [^{90}Y]DOTA-HBP and [^{90}Y]citrate, but the ratios of other tissues to osteogenic cells for [^{90}Y]DOTA-HBP were lower than those for [^{90}Y]citrate.

4. Discussion

Since bisphosphonates have exceptional affinity for hydroxyapatite, they have been used as carriers to deliver several classes of therapeutic agents to bone tissue [20]. In nuclear medicine, bisphosphonates function not only as carriers but also as ligands for radiometals such as ^{99m}Tc and $^{186/188}$Re in the cases of [^{99m}Tc]MDP, [^{99m}Tc]HMDP and [$^{186/188}$Re]HEDP [21,22]. Accordingly, the phosphonate groups in these complexes serve as both coordinating ligands and hydroxyapatite-binding functional groups, which might decrease the inherent accumulation of bisphosphonate in the bone. Besides, these complexes cannot be obtained as a single well-defined chemical species but as mixtures of short-chain and long-chain oligomers, which may reduce the efficacy of the radiopharmaceutical [23]. In the case of [^{186}Re]HEDP, since rhenium is more easily oxidized than technetium [24], in vivo decomposition of [^{186}Re]HEDP to $^{186}ReO_4^-$ was observed [25]. This resulted in delayed blood clearance and higher gastric uptake of radioactivity. Thus, to overcome these shortcomings, novel radiolabeled bisphosphonate compounds have been developed by conjugating stable mononuclear ^{99m}Tc- or ^{186}Re-chelating groups with bisphosphonate analogs [9,10,12,26–28]. Some of the compounds showed superior results in preclinical studies [9,26,28]. Therefore, we hypothesized that this strategy

Table 2
Biodistribution of radioactivity after intravenous administration of [^{90}Y]DOTA-HBP in mice

Tissue	Time after administration		
	10 min	60 min	180 min
Blood	0.87[a] (0.24)	0.07[a] (0.02)	0.03[a] (0.01)
Liver	0.41[a] (0.08)	0.27[a] (0.05)	0.18[a] (0.02)
Kidneys	4.74 (2.63)	0.94[a] (0.47)	0.44[a] (0.17)
Intestine	0.13[a] (0.03)	0.04[a] (0.01)	0.04[a] (0.02)
Spleen	1.13 (0.22)	0.98[a] (0.26)	0.68 (0.22)
Pancreas	0.27[a] (0.04)	0.03[a] (0.01)	0.03[a] (0.03)
Lungs	0.88[a] (0.15)	0.11[a] (0.03)	0.06[a] (0.04)
Heart	0.40[a] (0.06)	0.16[a] (0.23)	0.02[a] (0.01)
Stomach[b]	0.09[a] (0.03)	0.02[a] (0.01)	0.01[a] (0.00)
Femur	15.42 (1.35)	18.02[a] (4.14)	19.90[a] (2.02)
Muscle	0.21[a] (0.03)	0.04[a] (0.02)	0.02 (0.01)

Data are expressed as percent injected dose per gram of tissue. Each value represents the mean (S.D.) for five animals.
[a] Significant differences from [^{90}Y]citrate.
[b] Data are expressed as percent injected dose.

Table 3
Biodistribution of radioactivity after intravenous administration of [^{90}Y]citrate in mice

Tissue	Time after administration		
	10 min	60 min	180 min
Blood	2.92 (0.81)	1.26 (0.38)	0.22 (0.04)
Liver	1.15 (0.07)	1.43 (0.27)	2.47 (0.71)
Kidneys	3.69 (1.02)	3.17 (1.28)	7.10 (3.52)
Intestine	0.68 (0.08)	0.44 (0.05)	0.45 (0.12)
Spleen	1.14 (0.14)	0.61 (0.07)	0.60 (0.11)
Pancreas	1.29 (0.21)	0.53 (0.05)	0.19 (0.05)
Lungs	2.82 (0.66)	1.34 (0.15)	0.92 (0.19)
Heart	1.78 (0.16)	0.94 (0.09)	0.72 (0.18)
Stomach[a]	0.55 (0.05)	0.40 (0.07)	0.69 (0.38)
Femur	15.08 (2.43)	31.27 (2.93)	37.68 (5.35)
Muscle	1.57 (0.51)	0.32 (0.06)	0.34 (0.27)

Data are expressed as percent injected dose per gram of tissue. Each value represents the mean (S.D.) for five animals.
[a] Data are expressed as percent injected dose.

Table 4
Absorbed dose estimates of [^{90}Y]DOTA-HBP, [^{90}Y]citrate and [^{153}Sm]EDTMP

Organ	[^{90}Y]DOTA-HBP	[^{90}Y] Citrate	[^{153}Sm] EDTMP[a]
Osteogenic cells (mGy/MBq)	9.33E+00	1.21E+01	7.65E+00
Red marrow (mGy/MBq)	4.65E+00	6.05E+00	1.21E+00
Liver (mGy/MBq)	2.00E−03	5.87E−02	2.50E−02
Kidneys (mGy/MBq)	1.28E−02	2.18E−01	5.02E−02
Small intestine (mGy/MBq)	4.64E−04	1.60E−02	1.63E−02
Stomach (mGy/MBq)	4.38E−04	3.88E−02	1.17E−02
Spleen (mGy/MBq)	1.15E−02	1.42E−01	1.14E−02
Pancreas (mGy/MBq)	2.52E−04	4.96E−03	7.80E−03
Lungs (mGy/MBq)	2.76E−03	6.90E−02	1.49E−02
Muscle (mGy/MBq)	6.55E−04	1.50E−02	1.01E−02
Effective dose equivalent (mSv/MBq)	8.40E−01	1.13E+00	3.87E−01
Effective dose (mSv/MBq)	6.52E−01	8.71E−01	2.32E−01

[a] Each value was calculated from the data of the biodistribution study by Goeckeler et al. [19].

would be useful in the development of a novel ^{90}Y-labeled bone-seeking radiopharmaceutical, so we undertook to synthesize a novel [^{90}Y]DOTA-conjugated bisphosphonate.

Previously, development of a DOTA-conjugated bisphosphonate (BPAMD) for application in a magnetic resonance imaging (MRI) contrast agent as Gd(III) complex has been reported [29]. BPAMD does not have a hydroxyl group (α-OH group) at the central carbon of the bisphosphonate structure. The DOTA-HBP that we synthesized has an α-OH group. Previous studies of bisphosphonates suggest that the presence of the α-OH group affects the affinity for bone minerals [30,31]. In the design of radiometal complex-conjugated bisphosphonate derivatives, it has also been suggested that the α-OH group is effective in enhancing accumulation in the bone [10]. Accordingly, we suppose that DOTA-HBP might be designed by a more ideal structure-based drug design as a bone-seeking ligand.

Since DOTA-HBP contains not only a DOTA ligand site but also a bisphosphonate site, there is the possibility that ^{90}Y coordinates with the bisphosphonate moiety and not with the DOTA moiety. To ascertain that ^{90}Y is selectively complexed with only the DOTA moiety, the mixture containing DOTA and Compound (2) at equal mole concentrations was reacted under the same condition of the labeling reaction of DOTA-HBP. By RP-HPLC analysis of this reaction mixture, the ^{90}Y-labeled product was found to be identical to that obtained from the reaction of only DOTA with ^{90}Y. These findings suggest that ^{90}Y is chelated with the DOTA moiety in DOTA-HBP.

Contrary to our expectations, in stability experiments in plasma, the stability of [^{90}Y]DOTA-HBP was not so high. However, [^{90}Y]DOTA-HBP was nearly intact after 1 h of incubation in plasma. When this type of radiopharmaceutical is injected in vivo, some parts should rapidly accumulate in the bone, and the rest should be rapidly excreted in urine. Thus, it is supposed that the instability over the long term does not affect biodistribution. Actually, in biodistribution experiments, [^{90}Y]DOTA-HBP showed excellent selectivity for bone, as expected. [^{90}Y]Citrate showed a higher level of accumulation in the bone than [^{90}Y]DOTA-HBP, but [^{90}Y] citrate also accumulated in soft tissues. Consequently, the ratios of [^{90}Y]DOTA-HBP accumulation in the bone to that in soft tissues were significantly higher than those of [^{90}Y] citrate. We assumed that the pharmacokinetics of the [^{90}Y] DOTA-HBP complex might be so strongly affected by the DOTA-HBP ligand that the [^{90}Y]DOTA-HBP would show rapid clearance from the blood and soft tissue. In other words, complexes of DOTA-HBP with other metals might also show similar pharmacokinetics.

When bone affinity is compared with those of other bone-seeking agents measured in different species, the uptake value is expressed as %dose/g tissue×body weight in order to normalize the difference in the weight of the animals [32]. The corresponding value of [^{90}Y]DOTA-HBP in the femur at 1 h postinjection was 514%, while the value of [^{153}Sm] EDTMP, which was approved by the Food and Drug Administration for the treatment of painful bone metastases in 1997, was 707% (2 h; rats) [19] or 580% (24 h; rats) [33]. Since the uptake value of [^{90}Y]DOTA-HBP was only slightly less than that of [^{153}Sm]EDTMP, it is expected that [^{90}Y]DOTA-HBP could be of clinical use from the point of view of bone uptake. Moreover, soft-tissue clearance of

Table 5
Ratios between absorbed dose estimates for some organs and bone surfaces

Organ/osteogenic cells ratio	[^{90}Y] DOTA-HBP	[^{90}Y] Citrate	[^{153}Sm] EDTMP[a]
Red marrow/osteogenic cells	0.49839	0.50000	0.15817
Liver/osteogenic cells	0.00021	0.00485	0.00327
Kidneys/osteogenic cells	0.00137	0.01802	0.00656
Small intestine/osteogenic cells	0.00005	0.00132	0.00213
Stomach/osteogenic cells	0.00005	0.00321	0.00153
Spleen/osteogenic cells	0.00123	0.01174	0.00149
Pancreas/osteogenic cells	0.00003	0.00041	0.00102
Lungs/osteogenic cells	0.00030	0.00570	0.00195
Muscle/osteogenic cells	0.00007	0.00124	0.00132
Effective dose equivalent/osteogenic cells (Sv/Gy)	0.09003	0.09339	0.05059
Effective dose/ osteogenic cells (Sv/Gy)	0.06988	0.07198	0.03033

[a] Each value was calculated from the data of the biodistribution study by Goeckeler et al. [19].

Table 6
Biodistribution of radioactivity after intravenous administration of [^{99m}Tc] HMDP in mice

Tissue	Time after administration		
	10 min	60 min	180 min
Blood	1.63 (0.23)	0.15 (0.07)	0.07 (0.02)
Liver	0.48 (0.09)	0.14 (0.04)	0.13 (0.03)
Kidneys	10.78 (1.66)	5.69 (1.88)	0.85 (0.35)
Intestine	0.41 (0.05)	0.12 (0.02)	0.17 (0.04)
Spleen	0.46 (0.08)	0.11 (0.03)	0.07 (0.02)
Stomach[a]	0.23 (0.03)	0.15 (0.14)	0.19 (0.17)
Femur	16.87 (2.12)	19.65 (1.76)	19.21 (2.08)
Muscle	0.61 (0.15)	0.15 (0.06)	0.17 (0.12)

Data are expressed as percent injected dose per gram of tissue. Each value represents the mean (S.D.) for five animals.
[a] Data are expressed as percent injected dose.

Table 7
Femur/tissue ratios of [^{90}Y]DOTA-HBP, [^{153}Sm]EDTMP and [^{177}Lu] DOTMP

Tissue	[^{90}Y]DOTA-HBP[a]	[^{153}Sm]EDTMP[b]	[^{177}Lu]DOTMP[c]
Liver	70.0 (22.1)	137.8	32.5
Kidneys	26.7 (19.6)	25.3	12.1
Intestine	472.9 (87.8)	53.1	9.8
Stomach	1371.0 (737.7)	90.7	84.6

Data are expressed as the ratio of percent injected dose per gram of tissue.
[a] Each value represents the mean (S.D.) for five mice at 1 h postinjection.
[b] Each value was calculated using the data for rats at 2 h postinjection in Goeckeler et al. [19].
[c] Each value was calculated using the data for rats at 3 h postinjection in Das et al. [35].

[^{90}Y]DOTA-HBP could be comparable to that of [^{153}Sm]EDTMP because it was reported that [^{99m}Tc]MDP and [^{153}Sm]EDTMP showed no significant soft-tissue uptake [34], and the accumulation of [^{90}Y]DOTA-HBP in soft tissue was not high compared with [^{99m}Tc]HMDP (Tables 2 and 6). Meanwhile, the value (%dose/g tissue×body weight) of [^{177}Lu]1,4,7,10-tetraazacyclododecane-1,4,7,10-tetraamino-methylenephosphonate (DOTMP), which is currently under development for the treatment of painful bone metastases, was 1058% (3 h; rats) [35]. However, the ratios of bone to other tissues are 9.8 (intestine), 12.1 (kidney) and 32.5 (liver) (3 h; rats), respectively. These values are not large compared with those of [^{90}Y]DOTA-HBP and [^{153}Sm]EDTMP (Table 7). Thus, we do not suppose that [^{177}Lu]DOTMP is a complex that is superior to [^{90}Y]DOTA-HBP and [^{153}Sm]EDTMP from the point of view of biodistribution.

In dosimetry calculations, the ratios of the absorbed dose in soft tissues to that in osteogenic cells of [^{90}Y]DOTA-HBP were much lower than those of [^{90}Y]citrate, reflecting the results of the biodistribution experiments. These results were reflected in the values of effective dose equivalent and effective dose. However, in the case of the absorbed dose for red marrow, known as the dose-limiting factor of radiopharmaceuticals for palliation of metastatic bone pain, the ratios of the absorbed dose in red marrow to that in osteogenic cells were almost the same for [^{90}Y]DOTA-HBP and [^{90}Y]citrate. That is to say, both compounds might show similar degrees of myelosuppression, which is the most important side effect, in obtaining equal therapeutic effect. Because the radiation dose for bone marrow is highly influenced by the accumulation of radioactivity in the bone, improvement in the clearances of the blood and other tissues should contribute little to the radiation dose for red marrow. Meanwhile, although the ratios of the absorbed dose in soft tissues to that in osteogenic cells of [^{90}Y]DOTA-HBP were also lower than those of [^{153}Sm]EDTMP, [^{153}Sm]EDTMP has the advantage over [^{90}Y]DOTA-HBP in terms of the effective dose equivalent and effective dose. It is attributed to the difference in the radiation of red marrow. Namely, ^{153}Sm should be more appropriate than ^{90}Y as a radionuclide used in palliation therapy because the energy of the ^{90}Y β particles could be too high.

In conclusion, [^{90}Y]DOTA-HBP showed superior biodistribution characteristics as a bone-seeking agent and led to a decrease in the level of unnecessary radiation compared to [^{90}Y]citrate. Since the DOTA ligand forms a stable complex not only with ^{90}Y but also with lutetium (^{177}Lu), indium (^{111}In), gallium ($^{67/68}$Ga), gadolinium (Gd) and so on, complexes of DOTA-HBP with various metals could be useful as agents for palliation of metastatic bone pain, bone scintigraphy and MRI.

References

[1] Portenoy RK, Payne D, Jacobsen P. Breakthrough pain: characteristics and impact in patients with cancer pain. Pain 1999;81:129–34.

[2] Portenoy RK, Lesage P. Management of cancer pain. Lancet 1999;353: 1695–700.

[3] Mercadante S. Malignant bone pain: pathophysiology and treatment. Pain 1997;69:1–18.

[4] Arcangeli G, Giovinazzo G, Saracino B, D'Angelo L, Giannarelli D, Micheli A. Radiation therapy in the management of symptomatic bone metastases: the effect of total dose and histology on pain relief and response duration. Int J Radiat Oncol Biol Phys 1998;42:1119–26.

[5] Lewington VJ. Bone-seeking radionuclides for therapy. J Nucl Med 2005;46(Suppl 1):38S–47S.

[6] Kutzner J, Hahn K, Grimm W, Rosler HP, Eckmann A, Bender S. Yttrium-90–citrat zur schmerztherapie bei knochenmetastasen ([Yttrium–citrate for pain-therapy by bone metastases]). NUC Compact 1990;21:128–32.

[7] Rosch F, Herzog H, Plag C, Neumaier B, Braun U, Muller-Gartner HW, et al. Radiation doses of yttrium-90 citrate and yttrium-90 EDTMP as determined via analogous yttrium-86 complexes and positron emission tomography. Eur J Nucl Med 1996;23:958–66.

[8] Ogawa K, Mukai T, Arano Y, Hanaoka H, Hashimoto K, Nishimura H, et al. Design of a radiopharmaceutical for the palliation of painful bone metastases: rhenium-186-labeled bisphosphonate derivative. J Labelled Comp Radiopharm 2004;47:753–61.

[9] Ogawa K, Mukai T, Arano Y, Ono M, Hanaoka H, Ishino S, et al. Development of a rhenium-186-labeled MAG3-conjugated bisphosphonate for the palliation of metastatic bone pain based on the concept of bifunctional radiopharmaceuticals. Bioconjug Chem 2005;16:751–7.

[10] Ogawa K, Mukai T, Arano Y, Otaka A, Ueda M, Uehara T, et al. Rhemium-186-monoaminemonoamidedithiol-conjugated bisphosphonate derivatives for bone pain palliation. Nucl Med Biol 2006;33: 513–20.

[11] Ogawa K, Mukai T, Asano D, Kawashima H, Kinuya S, Shiba K, et al. Therapeutic effects of a ^{186}Re-complex-conjugated bisphosphonate for the palliation of metastatic bone pain in an animal model. J Nucl Med 2007;48:122–7.

[12] Uehara T, Jin ZL, Ogawa K, Akizawa H, Hashimoto K, Nakayama M, et al. Assessment of ^{186}Re chelate-conjugated bisphosphonate for the development of new radiopharmaceuticals for bones. Nucl Med Biol 2007;34:79–87.

[13] Ogawa K, Mukai T, Kawai K, Takamura N, Hanaoka H, Hashimoto K, et al. Usefulness of competitive inhibitors of protein binding for improving the pharmacokinetics of ^{186}Re-MAG3-conjugated bisphosphonate (^{186}Re-MAG3-HBP), an agent for treatment of painful bone metastases. Eur J Nucl Med Mol Imaging 2009;36:115–21.

[14] de Klerk JM, van Dieren EB, van het Schip AD, Hoekstra A, Zonnenberg BA, van Dijk A, et al. Bone marrow absorbed dose of rhenium-186-HEDP and the relationship with decreased platelet counts. J Nucl Med 1996;37:38–41.

[15] Liepe K, Hliscs R, Kropp J, Runge R, Knapp Jr FF, Franke WG. Dosimetry of ^{188}Re-hydroxyethylidene diphosphonate in human prostate cancer skeletal metastases. J Nucl Med 2003;44:953–60.

[16] Stabin MG, Sparks RB, Crowe E. OLINDA/EXM: the second-generation personal computer software for internal dose assessment in nuclear medicine. J Nucl Med 2005;46:1023–7.

[17] de Jong M, Bakker WH, Krenning EP, Breeman WA, van der Pluijm ME, Bernard BF, et al. Yttrium-90 and indium-111 labelling, receptor binding and biodistribution of [DOTA0,D-Phe1,Tyr3]octreotide, a promising somatostatin analogue for radionuclide therapy. Eur J Nucl Med 1997;24:368–71.

[18] Paganelli G, Zoboli S, Cremonesi M, Bodei L, Ferrari M, Grana C, et al. Receptor-mediated radiotherapy with ^{90}Y-DOTA-D-Phe1-Tyr3-octreotide. Eur J Nucl Med 2001;28:426–34.

[19] Goeckeler WF, Edwards B, Volkert WA, Holmes RA, Simon J, Wilson D. Skeletal localization of samarium-153 chelates: potential therapeutic bone agents. J Nucl Med 1987;28:495–504.

[20] Zhang S, Gangal G, Uludag H. 'Magic bullets' for bone diseases: progress in rational design of bone-seeking medicinal agents. Chem Soc Rev 2007;36:507–31.